

**ROCK SALT MECHANICAL BEHAVIOR UNDER
CYCLIC LOADING WITH CONSTANT
MEAN STRESSES**



**A Thesis Submitted in Partial Fulfillment of the Requirements for the
Degree of Doctor of Philosophy of Engineering in Civil,
Transportation and Geo-resources Engineering
Suranaree University of Technology
Academic Year 2019**

พฤติกรรมเชิงกลศาสตร์ของเกลือหินภายใต้แรงกดแบบวัฏจักร
ด้วยความเค้นเฉลี่ยคงที่



วิทยานิพนธ์นี้เป็นส่วนหนึ่งของการศึกษาตามหลักสูตรปริญญาวิศวกรรมศาสตรดุษฎีบัณฑิต
สาขาวิชาวิศวกรรมโยธา ขนส่ง และทรัพยากรธรณี
มหาวิทยาลัยเทคโนโลยีสุรนารี
ปีการศึกษา 2562

ROCK SALT MECHANICAL BEHAVIOR UNDER CYCLIC LOADING WITH CONSTANT MEAN STRESSES

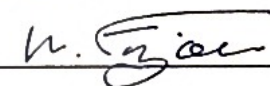
Suranaree University of Technology has approved this thesis submitted in partial fulfillment of the requirements for the Degree of Doctor of Philosophy.

Thesis Examining Committee



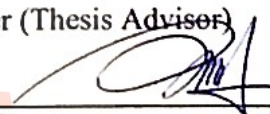
(Assoc. Prof. Dr. Pomkasem Jongpradist)

Chairperson



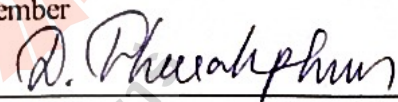
(Prof. Dr. Kittitep Fuenkajorn)

Member (Thesis Adviser)



(Asst. Prof. Dr. Akkhapun Wannakomol)

Member



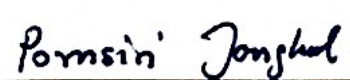
(Asst. Prof. Dr. Decho Phueakphum)

Member



(Asst. Prof. Dr. Prachya Tepnarong)

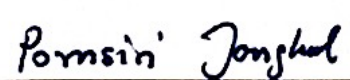
Member





(Assoc. Prof. Flt. Lt. Dr. Kontorn Chamniprasart)

Vice Rector for Academic Affairs
and Internationalization



(Assoc. Prof. Dr. Pornsiri Jongkol)

Dean of Institute of Engineering

กิตติศักดิ์ เต็งผั้วแก้ว : พฤติกรรมเชิงกลศาสตร์ของเกลือหินภายใต้แรงกดแบบวัฏจักรด้วยความเค้นเฉลี่ยคงที่ (ROCK SALT MECHANICAL BEHAVIOR UNDER CYCLIC LOADING WITH CONSTANT MEAN STRESSES)

อาจารย์ที่ปรึกษา : ศาสตราจารย์ ดร.กิตติเทพ เฟื่องขจร, 107 หน้า.

งานวิจัยนี้ได้ดำเนินการทดสอบ การกดแบบวัฏจักรในสามแกนภายใต้ความเค้นเฉลี่ยคงที่ เพื่อคาดคะเนการเปลี่ยนรูปร่างเชิงเวลาของเกลือหินสำหรับประยุกต์ใช้ในการกักเก็บพลังงาน อากาศอัด โดยนำตัวอย่างเกลือหินรูปปริซึมมาทดสอบภายใต้ความดันล้อมรอบที่ผันแปรจากร้อยละ 20 ถึงร้อยละ 90 ของความเค้นในภาคสนาม และความเค้นในแนวตั้งจากความลึกในช่วง 250 ถึง 400 เมตร โดยใช้สัดส่วนการขุดเจาะเทียบเท่าจากร้อยละ 30 ถึงร้อยละ 60 ในช่วงระหว่างการกดแบบวัฏจักรความเครียดในสภาวะอัตราการคืบคงที่ได้มีการคำนวณความเครียดเฉือนในสามแกนตลอดช่วงเวลาการทดสอบ ซึ่งกฎการคืบแบบยกกำลังและการคืบแบบ Burgers มีความสอดคล้องอย่างเป็นเหตุเป็นผลกับข้อมูลจากความเครียด เวลา และความเค้นที่วัดได้ การกดแบบวัฏจักรจะให้ค่าความเครียดสูงกว่าการกดแบบสถิตสำหรับทุกความลึกและทุกสัดส่วนการขุดเจาะ ซึ่งบอกเป็นนัยว่า การยุบตัวของเสาค้ำยันเกลือหินจะมีค่าสูงภายใต้การกดแบบวัฏจักรเมื่อเทียบกับการรับแรงกดแบบสถิต ค่าความหนืดเชิงพลาสติกในสภาวะความเค้นเฉลี่ยคงที่มีค่าประมาณ 20 GPa.day ต่ำกว่าภายใต้ความเค้นล้อมรอบคงที่ พลังงานความเครียดที่จุดแตกของเกลือหินที่ได้จากงานวิจัยที่เกี่ยวข้อง ได้นำมาใช้ในการคาดคะเนกำลังกดที่ขึ้นกับเวลาของตัวอย่างเกลือหิน ภายใต้การกักเก็บพลังงาน สรุปได้ว่าเสถียรภาพของเกลือหินจะลดลงเมื่อมีการเพิ่มความเครียดเฉือนในสามแกน (เพิ่มสัดส่วนการขุดเจาะและความลึก)

สาขาวิชา เทคโนโลยีธรณี

ปีการศึกษา 2562

ลายมือชื่อนักศึกษา กิตติศักดิ์ เต็งผั้วแก้ว

ลายมือชื่ออาจารย์ที่ปรึกษา ดร.กิตติเทพ เฟื่องขจร

KITTISAK TENGPAKWAEN : ROCK SALT MECHANICAL BEHAVIOR
UNDER CYCLIC LOADING WITH CONSTANT MEAN STRESSES.

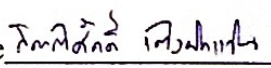
THESIS ADVISOR : PROF. KITTITEP FUENKAJORN, Ph.D., P.E., 107 PP.

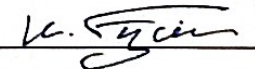
CREEP/STRAIN ENERGY/POTENTIAL CREEP LAW/BURGERS MODEL/
EQUIVALENT EXTRACTION RATIO

Triaxial cyclic loading tests under constant mean stresses have been performed to predict the time-dependent deformation of rock salt for a compressed-air energy storage application. Rectangular prisms of salt are subjected to confining pressures vary from 20% to 90% of the in-situ stresses for depths ranging from 250 to 400 m with equivalent extraction ratios from 30 to 60%. During cyclic loading, the steady-state creep strains are calculated in terms of the octahedral shear strains as a function of time. Both potential creep law and Burgers model fit reasonably well to the strain, time and stress data. The cyclic loading induces a higher creep strain than that of the static loading for all depths and extraction ratios, suggesting that long-term creep deformations of salt pillars may be greater under cyclic loading than under static loading. The visco-plastic coefficients obtained under constant mean stress are about 20 GPa·day lower than those under constant confining pressure. The distortional strain energy at failure from relevant research is used to predict the time-dependent strengths of the creeping salt specimens. Under storage operation, stability of salt decreases with increasing octahedral shear stresses (equivalent extraction ratio and depth).

School of Geotechnolgy

Academic Year 2019

Student's Signature 

Advisor's Signature 

ACKNOWLEDGMENTS

I wish to acknowledge the funding support from Suranaree University of Technology (SUT).

I would like to express thanks to Prof. Dr. Kittitep Fuenkajorn, thesis advisor, who gave a critical review. I appreciate his encouragement, suggestions, and comments during the research period. I would like to express thanks to Assoc. Prof. Dr. Pornkasem Jongpradist, Asst. Prof. Dr. Akkhapun Wannakomol, Asst. Prof. Dr. Decho Phueakphum and Asst. Prof. Dr. Prachya Tepnarong for their valuable suggestions and comments on my research works as thesis committee members. Grateful thanks are given to all staffs of Geomechanics Research Unit, Institute of Engineering who supported my work.

Finally, I most gratefully acknowledge my parents and friends for all their supported throughout the period of this study.

Kittisak Tengpakwaen

TABLE OF CONTENTS

	Page
ABSTRACT (THAI).....	I
ABSTRACT (ENGLISH).....	II
ACKNOWLEDGEMENTS.....	III
TABLE OF CONTENTS.....	IV
LIST OF TABLES.....	VII
LIST OF FIGURES.....	VIII
SYMBOLS AND ABBREVIATIONS.....	XII
CHAPTER	
I INTRODUCTION.....	1
1.1 Background and rationale.....	1
1.2 Research objectives.....	2
1.3 Research methodology.....	2
1.3.1 Literature review.....	2
1.3.2 Sample preparation.....	3
1.3.3 Triaxial cyclic loading tests.....	3
1.3.4 Mathematical relations.....	3
1.3.5 Prediction of long-term salt strength.....	3
1.3.6 Discussions, conclusion and thesis writing.....	4

TABLE OF CONTENTS (Continued)

	Page
1.4 Scope and limitations.....	5
1.5 Thesis contents.....	5
II LITERATURE REVIEW.....	6
2.1 Introduction.....	6
2.2 Cyclic loading test.....	6
2.3 Compressed-air energy storage.....	12
III LABORATORY TESTS.....	16
3.1 Introduction.....	16
3.2 Sample preparation.....	16
3.3 Test apparatus and method.....	18
IV TEST RESULTS.....	25
4.1 Introduction.....	25
4.2 Static loading test results.....	25
4.3 Cyclic loading test results.....	26
V ANALYSIS OF TEST RESULTS.....	36
5.1 Introduction.....	36
5.2 Octahedral shear strain.....	36
5.3 Calibration of creep model parameters.....	39
5.3.1 Burgers model.....	40
5.3.2 Potential creep law.....	47

TABLE OF CONTENTS (Continued)

	Page
VI TIME-DEPENDENT STRENGTH OF SALT UNDER CYCLIC LOADING	55
6.1 Introduction.....	55
6.2 Strain energy density calculation.....	55
6.3 Long-term salt strength based on potential law.....	57
6.4 Long-term salt strength based on Burgers model.....	65
6.5 Comparisons of long-term salt strengths.....	66
VII DISCUSSIONS AND CONCLUSIONS	74
7.1 Discussions.....	74
7.2 Conclusions.....	78
7.3 Recommendations for future studies.....	81
REFERENCES.....	82
BIOGRAPHY.....	91

LIST OF TABLES

Table	Page
3.1 Salt specimens prepared for triaxial cyclic loading tests.....	18
3.2 Loading conditions for static loading test.....	22
3.3 Loading conditions for cyclic loading test.....	23
5.1 Calibration results of Burgers parameters.....	46
5.2 Calibration results of Potential law parameters.....	54
5.3 Creep parameter of static and cyclic loading.....	54
6.1 Predictions of time at which failure occurs based on potential law.....	64
6.2 Burgers parameters for static and cyclic loadings.....	68
6.3 Predictions of time at failure occurs based on Burgers model.....	73

LIST OF FIGURES

Figure	Page
1.1 Research methodology.....	4
2.1 Cross section through the Bostock No. 5 panel showing model (Swift and Redish, 2005).....	14
2.2 Maximum principal stress distribution around central two rooms.....	14
3.1 Salt specimen is dry-cut by cutting device.....	17
3.2 Some rectangular specimens of salt used in triaxial static and cyclic loading testing.....	17
3.3 Polyaxial load frame (Fuenkajorn et al., 2012) used in triaxial cyclic loading testing.....	19
3.4 Tributary area concept. (Farmer and Gilbert, 1984).....	20
3.5 Cyclic loading paths as function of time.....	24
4.1 Axial and lateral strains as a function of time for static loading under maximum axial stresses of 7.50, 8.75 and 13.13 MPa (for $e = 30, 40$ and 60%) at equivalent depth of 250 m.....	28
4.2 Axial and lateral strains as a function of time for static loading under maximum axial stresses of 9.00, 10.50 and 15.75 MPa (for $e = 30, 40$ and 60%) at equivalent depth of 300 m.....	29
4.3 Axial and lateral strains as a function of time for static loading under maximum axial stresses of 10.50, 12.25 and 18.38 MPa (for $e = 30, 40$ and 60%) at equivalent depth of 350 m.....	30

LIST OF FIGURES (Continued)

Figure	Page
4.4	Axial and lateral strains as a function of time for static loading under maximum axial stresses of 12.00, 14.00 and 21.00 MPa (for $e = 30, 40$ and 60%) at equivalent depth of 400 m.....31
4.5	Axial and lateral strains as a function of time simulating storage depth of 250 m ($\sigma_v = 5.25$ MPa).....32
4.6	Axial and lateral strains as a function of time simulating storage depth of 300 m ($\sigma_v = 6.30$ MPa).....33
4.7	Axial and lateral strains as a function of time simulating storage depth of 350 m ($\sigma_v = 7.35$ MPa).....34
4.8	Axial and lateral strains as a function of time simulating storage depth of 400 m ($\sigma_v = 8.40$ MPa).....35
5.1	Octahedral shear strain as a function of elapse time for depth of 250 m.....37
5.2	Octahedral shear strain as a function of elapse time for depth of 300 m.....38
5.3	Octahedral shear strain as a function of elapse time for depth of 350 m.....38
5.4	Octahedral shear strain as a function of elapse time for depth of 400 m.....39
5.5	Modular components of Burgers model.....40
5.6	Octahedral shear strain as a function of time and curves fitting with Burgers model under octahedral shear stresses at depth 250 m.....42
5.7	Octahedral shear strain as a function of time and curves fitting with Burgers model under octahedral shear stresses at depth 300 m.....43

LIST OF FIGURES (Continued)

Figure	Page
5.8	Octahedral shear strain as a function of time and curves fitting with Burgers model under octahedral shear stresses at depth 350 m.....44
5.9	Octahedral shear strain as a function of time and curves fitting with Burgers model under octahedral shear stresses at depth 400 m.....45
5.10	Burgers parameters as a function of maximum octahedral shear stress.....47
5.11	Octahedral shear strain as a function of time and curves fitting with potential law at depth 250 m.....50
5.12	Octahedral shear strain as a function of time and curves fitting with potential law at depth 300 m.....51
5.13	Octahedral shear strain as a function of time and curves fitting with potential law at depth 350 m.....52
5.14	Octahedral shear strain as a function of time and curves fitting with potential law at depth 400 m.....53
6.1	Distortional strain energy at failure as a function of mean stress by Junthong et al. (2016).....57
6.2	Calculated distortional strain energy as a function of testing time based on potential law for depth of 250 m.....59
6.3	Calculated distortional strain energy as a function of testing time based on potential law for depth of 300 m.....60
6.4	Calculated distortional strain energy as a function of testing time based on potential law for depth of 350 m.....61

LIST OF FIGURES (Continued)

Figure	Page
6.5	Calculated distortional strain energy as a function of testing time based on potential law for depth of 400 m.....62
6.6	Prediction of time-dependent strength based on potential law, comparing static with cyclic loading conditions.....63
6.7	Calculated distortional strain energy as a function of testing time based on Burgers model for depth of 250 m.....68
6.8	Calculated distortional strain energy as a function of testing time based on Burgers model for depth of 300 m.....69
6.9	Calculated distortional strain energy as a function of testing time based on Burgers model for depth of 350 m.....70
6.10	Calculated distortional strain energy as a function of testing time based on Burgers model for depth of 400 m.....71
6.11	Predictions of time-dependent strength based on Burgers model, comparing static with cyclic loading conditions.....72
7.1	Comparison of η_1 calibrated from cyclic loading with constant σ_3 by Archeeploha and Fuenkajorn (2013).....79

SYMBOLS AND ABBREVIATIONS

ρ	=	In-situ stress gradient of overburden
ε_1	=	Major principal strain
ε_3	=	Minor principal strain
$\varepsilon_{\text{axial}}$	=	Axial strain
ε^c	=	Time-dependent plastic strain
ε^e	=	Elastic strain
$\varepsilon_{\text{lateral}}$	=	Lateral strain
$\gamma_{\text{oct}}(t)$	=	Octahedral shear strain as a function of time
γ_{oct}	=	Octahedral shear strain
ε^T	=	Total strain
$\dot{\varepsilon}$	=	First order partial derivatives of strain respect to time
$\ddot{\varepsilon}$	=	Second order partial derivatives of strain respect to time
$\dot{\sigma}$	=	First order derivatives of stress respect to time
$\ddot{\sigma}$	=	Second order derivatives of stress respect to time
E	=	Elastic modulus
e	=	Equivalent extraction ratio
E_1	=	The elastic modulus
E_2	=	The spring constant in visco-elastic phase
G	=	The shear modulus
H	=	Mine depth

SYMBOLS AND ABBREVIATIONS (Continued)

P_{\max}	=	Maximum pressure (during injection)
P_{\min}	=	Minimum pressure (during withdrawal)
t	=	Time
W_d	=	Distortional strain energy
$W_{d,f}$	=	Distortional strain energy at failure
W_o	=	Pillar width of a square
W_p	=	Room width of a square
ν	=	Poisson's ratio
$\sigma_{1,\text{with}}$	=	Axial stress (withdrawal condition)
σ_3	=	Confining pressure
σ_m	=	Mean stress
σ_p	=	Equivalent pillar stress
σ_v	=	Vertical stress
β	=	Empirical constants
γ	=	Empirical constants
η_1	=	Visco-plastic viscosity
η_2	=	Visco-elastic viscosity
κ	=	Empirical constants
$\tau_{\text{oct,max}}$	=	Maximum octahedral shear stress
$\tau_{\text{oct,min}}$	=	Minimum octahedral shear stress

CHAPTER I

INTRODUCTION

1.1 Background and rationale

Abandoned salt mines can be developed as a compressed-air energy storage (CAES) facility to take an advantage of the underground space after excavation is completed. Rock salt has been widely recognized as the most suitable for storage of energy by compressed-air due to its low permeability. Salt mine normally has a high mechanical stability which can be achieved when it is properly designed. During storage operation the mine openings may not have to maintain high internal pressure, whereas the salt caverns must keep minimum internal pressure at least 20-30% of the in-situ stress at the casing shoe. One of the problems involving in the compressed-air storage in the mine openings is the effect of stress changes in the supported pillars due to the injection-withdrawal cycles. The conventional creep tests where the salt specimens are subjected to constant stresses may not truly represent the actual salt behavior under the storage conditions. Even though the effects of cyclic loading on the time-dependent behavior of salt have been recognized and studied, the effects of the actual storage conditions (i.e. cyclic loading under constant mean stress) around salt mine on the creep behavior of the rock salt have never been assessed.

1.2 Research objectives

This study is primarily aimed at determining the effects of the repeated cycles of mechanical loadings on the time-dependent deformation of rock salt and to evaluate the long-term stability of salt pillars for compressed-air storage (CAES) technology in abandoned salt mines by laboratory testing. The triaxial cyclic loading test under constant mean stresses is performed to simulate the behavior of salt pillars under storage operation. The axial cyclic stresses vary from 30% to 70% of the salt strength with confining pressures vary from 20% to 90% of the in-situ stress. The calculations are made for the depths from 250, 300, 350 to 400 m. At each depth, equivalent the extraction ratios are varied from 30, 40 to 60%. This selected range of testing stresses covers those likely occurred in the planned operation. Creep model parameters are used to simulate the salt deformability and strength under mechanical cyclic loading. The results are used to assess the stability of salt pillars under compressed-air storage condition.

1.3 Research methodology

The research methodology shown in Figure 1.1 comprises 7 steps; including literature review, sample preparation, laboratory testing, mathematical relations, long-term stability of salt under cyclic loading, discussions and conclusions and thesis writing.

1.3.1 Literature review

Literature review is carried out to understand the CAES technology in rock salt, especially those related to behavior of rock salt subjected to cyclic loading.

The sources of information are from text books, journals, technical reports and conference papers.

1.3.2 Sample preparation

Rock salt samples have been obtained from ASEAN Potash Mining Co., Ltd. (APMC) from Khorat basin, northeast of Thailand. The salt specimens are rectangular prisms with nominal dimensions of $54 \times 54 \times 108 \text{ mm}^3$ for cyclic loading tests. Preparations of these samples follows as much as practical the American Society for Testing and Materials Standard Practice (ASTM D4543). Over 12 specimens have been used for this study.

1.3.3 Triaxial cyclic loading tests

The triaxial cyclic loading tests are performed under constant mean stresses such that the rock salt specimen is simulated under actual salt pillar loading condition for compressed-air storage. The testing is conducted using a polyaxial load frame (Fuenkajorn and Kenkhunthod, 2010) to apply axial and lateral stresses to the salt specimens. The axial stress varies from 30% to 70% of the salt strength with confining pressures varying from 10% to 90% of the in-situ stress.

1.3.4 Mathematical relations

The results are used to describe the deformability of salt rock specimens with time dependency under mechanical cyclic loads. The Burgers model and potential creep law are used to fit with the test results. Test data are used to calibrate the elastic, visco-elastic and visco-plastic parameters of the models.

1.3.5 Prediction of long-term salt strength

The long-term suitability of salt pillars are studied by extrapolation of the creep models for various depths, pillar stresses and operation durations.

1.3.6 Discussions, conclusions and thesis writing

Discussions are made to analyze the impacts of the mechanical cyclic loads on the pillars stability. All research activities, methods, and results are documented and compiled in the thesis. The research or findings will be published in the conference proceedings or journals.

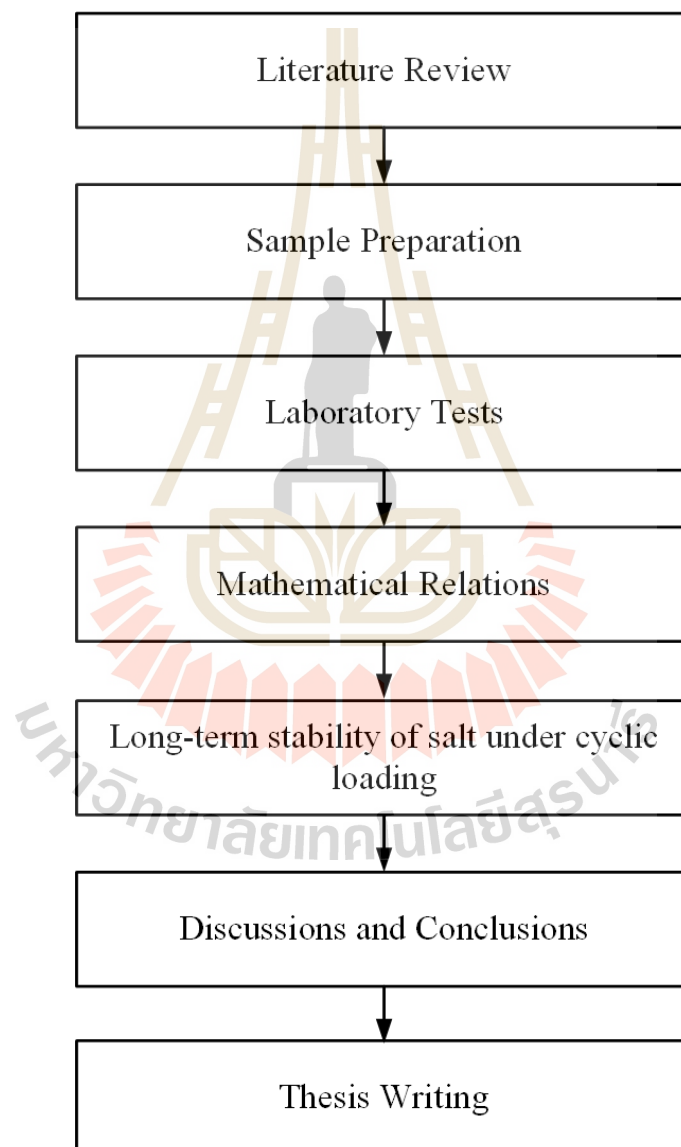


Figure 1.1 Research methodology.

1.4 Scope and limitations

Given below are the scope and limitations of this study.

1. All testing is conducted on rock salt specimens obtained from Maha Sarakham formation. The rock salt is relatively pure halite with slight amount (less than 1-2%) of anhydrite, clay minerals and ferrous oxide.

2. All cyclic loading tests are performed up to 21 days (or 21 cycles).

3. Series of triaxial cyclic loading tests are performed with the applied axial stresses varying from 30% to 70% of salt strength and confining pressures varying from 20% to 90% of the in-situ stress. The test procedure follows the ASTM standard practice, as much as practical.

4. The long-term mechanical properties of rock salt pillars are estimated from the laboratory test results.

1.5 Thesis contents

Chapter I describes the background and rationale, the objectives, the methodology and scope and limitations of the research. **Chapter II** presents results of the literature review on cyclic loading tests and compressed-air energy storage technology. **Chapter III** describes the salt sample preparation and laboratory testing. **Chapter IV** describes test results. **Chapter V** shows the creep calibrations. **Chapter VI** determines long-term stability of salt pillars. **Chapter VII** presents the discussions, conclusions, and recommendations for future studies.

CHAPTER II

LITERATURE REVIEW

2.1 Introduction

Literature review has been carried out to improve an understanding the time-dependent behavior and mechanical properties of rock salt. Literatures related to the compressed-air energy storage technology in rock salt beds and domes have been reviewed in this research. This research emphasizes the mechanical performance of rock salt formations to be applied in energy storage technology. The related knowledge is categorized into two groups: 1) cyclic loading tests and 2) compressed-air energy storage technology.

2.2 Cyclic loading test

Effect of cyclic loading can cause damage to engineering structures, for example, dam, road, bridge foundations and tunnels. The causes could be from earthquake, traffic, blasting and the process of compressed and released air in and out of the cavern, etc. Civil engineering materials, such as steels, concrete or soil can be affected by cyclic loading. The aim of the cyclic loading test in rock salt is to understand the duration of structures under repeat loading and to apply the results in designing air controlling systems during CAES operation. A rock salt cavern is subjected to pressure fluctuation. The pressures will be high and low in according to

its operation. The duration can be referred from the number of pressurized cycles before cracking occurs.

Thoms et al. (1980) performed low frequency triaxial cyclic loading by using the loading condition of the CAES in rock salt cavern. The change of temperature in cycle can induce creep in rock salt. Frequency affects the behavior of rock salt. Different frequency causes difference in number of cycles that induces failure. Number of cycles that cause failure under higher frequency is more than the number of cycles in the lower frequency. And under higher stress (fatigue stress), the loading cycle that causes failure is less than that in the lower stress.

The cyclic loading test performed by Passaris (1982) on rock salt to design compressed-air energy storage cavern. The tests were performed at low frequency (0.1 Hz). The applied load was imitated from the up-down pressures in rock salt cavern. The relationship between the fatigue strength (S) and the fatigue life (number of cycles causing failure-N): $S = 1.91N^{-0.05}$. The rock salt can soften by cyclic loading and the elastic modulus decreases as the number of cycles increase. The test reveals that the fatigue stress limit of rock salt is at 60% of the uniaxial compressive strength. The cavern pressure should be maintained higher than 55% of the rock salt strength.

Gehle and Thoms (1986) studied the change in acoustic emission (AE) characteristics causing by cyclic loading in rock salt cavern. The result from the test showed that the AE signal pattern increased as the pressure in the drilled holed increased. This means that cracks have developed. The summary indicates that the AE-method can measure the change in rock salt property which is affected by the

cyclic loading and can indicate the cracks development as increasing the number of loading cycles.

Thoms and Gehle (1982) study the effects of cyclic loading and changing of temperature on rock salt. Creep in rock salt from the cyclic loading test depends on the difference between the minimum and maximum loading. Changes of temperature in the cavern affects the salt creep. If the cavern were constructed at the depth of approximately 900 m, temperature would have a significant effect. The cyclic loading influencing factor is the magnitude of up-and down- stress (Haimson and Kim, 1972). If the difference between the up and down-stress is low, the permanent strains will be low. For a large difference in up and down-stress, the failure occurs at the lesser number of loading. Frequency has an influence on the cyclic loading test, the number of cycles causing failure is higher as the frequency increases (Atterwell and Farmer, 1973; Ishizuka and Abe, 1990). Crystal size affects the cyclic loading. Strengths of the fine-grained rock salt are higher than that of the coarse-grained rock. The number of cycle causing failure in fine-grained rock is then higher (Burdine, 1963); Water condition and confining pressure have an influence on the cyclic loading. Creep deformation under wet condition will be higher than in dry condition. The test under confining pressure results in higher number of loading cycles causing failure (Ishizuka and Abe, 1990) as compared to the unconfined test. Characteristics of creep deformation from cyclic loading test are the same as the creep deformation from the static creep test (Ishizuka and Abe, 1990).

When the specimen is subjected to loading and unloading, the fatigue occurs and consequently, the ultimate strength decreases (Mogi, 1962; Burdine, 1963; Hardy and Chugh, 1970; Haimson and Kim, 1972; Haimson, 1972; Atterwell and Farmer,

1973; Tharp, 1973; Kim, 1973; Fuenkajorn and Daeman, 1988). Results from cyclic loading test can be explained in terms of relationship between stress, strain and number of cycles (fatigue life).

Cristescu and Hunsche (1996) carry out the uniaxial creep test at various temperatures from 22 °C to 630 °C. The results show that under higher temperature, salt behavior is plastic due to higher ductility of salt. The methods of creep test can be applied in a multi- step creep test (Hamami et al., 1996; Allemandou and Dusseault, 1996), which carried out the uniaxial creep test, but the applied constant load is maintained to allow creep to occur, and then systematically increases another step of load after creep has occurred for a period of time. The multi-step uniaxial creep test can decrease the amount of specimen to be used in each step or stress level.

Cyclic loading tests performed by Fuenkajorn and Phueakphum (2010) on Maha Sarakham salt show that the number of loading cycles increases as the compressive strength decreases. The elastic modulus decreases during the first few cycles and tends to remain constant until failure. It is independent of maximum loads. Axial strain–time curves compiled from loci of the maximum load show creep behavior similar to that under static loading. In the steady-state creep phase, the visco-plastic coefficients are about an order of magnitude lower than those under static loading. The visco-plasticity decreases with increasing loading frequency.

Ma et al. (2013) study the mechanical properties of rock salt under triaxial cyclic loading. The elastic modulus decreases with increasing loading cycles. The modulus degradation depends on confining pressure and deviatoric stress. The confining pressure effect on the creep behavior under cyclic loading is similar to that

under static loading. The strain-hardening and ductile behavior are shown after a certain number of loading cycles.

Song et al. (2013) determine the fatigue life on rock salt. The testing includes uniaxial and triaxial cyclic loading tests under different stress amplitudes. The fatigue limit equal to 75% of the compressive strength. The results can be applied to design the pressure limits of gas injection and production of gas storage in salt.

Roberts et al. (2015) assess the effect of cyclic on rock salt from the Avery Island Mine. Cyclic loading does not make the salt more prone to dilation than static loading. Testing has only been conducted on a limited number of small crystal salt specimens with few impurities from the Avery Island Mine and additional test condition variables, such as frequency and duration of the cyclic loading, could be considered

Plangklang et al. (2017) perform four-point bending under cyclic loading tests. The induced maximum tensile stresses range from 1.21 to 3.20 MPa. The permanent strain increase and accumulates from each cycle until failure. Relation between the loading cycles (N) and fatigue tensile strength (S) indicate that the effect of frequency is relatively small. Elastic modulus of salt derived from the cyclic loading decrease as the loading cycles increases.

Kaewpuang et al. (2018) investigate cyclic loading effect on tensile strength of rock salt for the design of underground energy storage. The tensile strength reduces with increasing loading cycles and tends to be insensitive to the loading frequencies. The fatigue (S-N) curves can be represented by a logarithm relations. The loading frequencies have small effect to the fatigue strengths. The linear relation between the distortional and mean strain energy at failure is obtained which can describe the

fatigue tensile strength of salt under various loading paths and frequencies. The findings suggest that the roof of gas storage caverns in rock salt that subjects to cycles of compression-to-tension stresses would have fatigue strength of about half of those determined by the conventional cyclic tension test.

From the test that have been performed by many researchers in both laboratory and field, the responses of the cyclic loading test are in the same manner and can be summarized as follows:

1) The cyclic loading influencing factor is the magnitude of up-and down-stress (Haimson and Kim, 1972). If the difference between the up and down-stress is low, the permanent strains will be low.

2) Frequency has a small influence on the cyclic loading test, the number of cycles causing failure is higher as the frequency increases (Atterwell and Farmer, 1973; Ishizuka and Abe, 1990).

3) Crystal size affects the impact of cyclic loading. The loading cycles causing failure in fine-grained rock is then higher (Burdine, 1963).

4) Water condition and confining pressure have an influence on the cyclic loading. Creep deformation under wet condition will be higher than in dry condition. The test under confining pressure results in higher number of loading cycles causing failure (Ishizuka and Abe, 1990) as compared to the unconfined test.

5) Characteristics of creep deformation from cyclic loading test are the same as the creep deformation from the static creep test. (Ishizuka and Abe, 1990).

2.3 Compressed-air storage

The first compressed air energy storage (CAES) in the world is the Huntorf Plant in Germany which was started in 1978 (Crotogino et al., 2001). The caverns are at 650 meters deep. The constant volume system is employed to reconvert the compressed air to produce electricity. The maximum allowable pressure in the cavern is 70 bar. The minimum cavern pressure is as low as 20 bar. The same technology has been also used in McIntosh, Alabama since 1991 with the power capacity of 110 MW.

Results from many researches indicate that rock salt has higher efficiency for storage of compressed air than other rock types. Katz and Lady (1976), Change et al. (1980), and DeLong et al. (1989) summarize the application of CAES technology. Design and analysis of the solution storage cavern have been comprehensively studied in United States and Germany (Serata et al., 1989; Thoms and Martinez, 1978; Gehle and Thoms, 1986; Wittke et al., 1980; Fuenkajorn and Daemen, 1992; Fuenkajorn and Serata, 1992). Many researchers from various organizations have studied the mechanics and geology of the underground caverns for CAES in rock salt deposits and salt domes.

Serata et al. (1989) analyzed the geomechanical stability of salt dome in McIntosh, in the South of Alabama for the compressed air storage. The analysis was done by a computer model. Results from the analysis were used to assess the long-term effects on rock salt around the cavern. The analysis was also emphasized on the deformation of the cavern wall, stress distribution, the subsidence rates of ground surface, and the convergence of the cavern.

Electric Power Research Institute (EPRI), has conducted comprehensive research and developed the CAES technology. Various aspects have been studied and

continually developed, for example, the design of an underground cavern in rock salt deposits (EPRI, 1990a; 1990b; 1990c; 1992a; 1992b; 1992c; 1994a; 1994b), design of power generator for CAES (EPRI, 1994c; 1994d; 1997; 1999), economic assessment (EPRI, 1986; 1999), and CAES for other types of underground media.

Swift and Reddish (2005) presented simulations of the room and pillar of salt mine by used FLAC software. The model is reproduced in Figure 2.1. The principal load bearing elements are the pillars. Figure 2.2 shows the principal stress around the central two rooms and within the adjacent pillars. The redistribution of stresses is concentrated in the rock close to the mine excavation. The influence of the excavation reduces with increasing distance from the mine voids. The central part of the immediate roof of the room shows stress concentrations of 4 MPa. Stress concentrations increase towards the room corners. Safety factors for the central pillar and adjacent rooms have been calculated as a means of illustrating the relative stability of the mine structures. Strength/stress ratios of 3 are shown in the side walls and immediate roof this would be considered to indicate very stable conditions in mining situations.

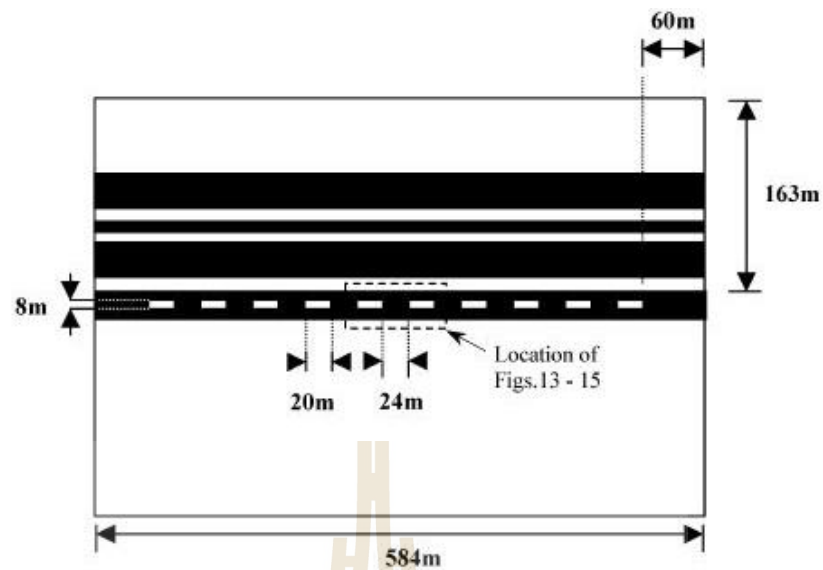


Figure 2.1 Cross section through the Bostock No. 5 panel showing model (Swift and Redish, 2005).

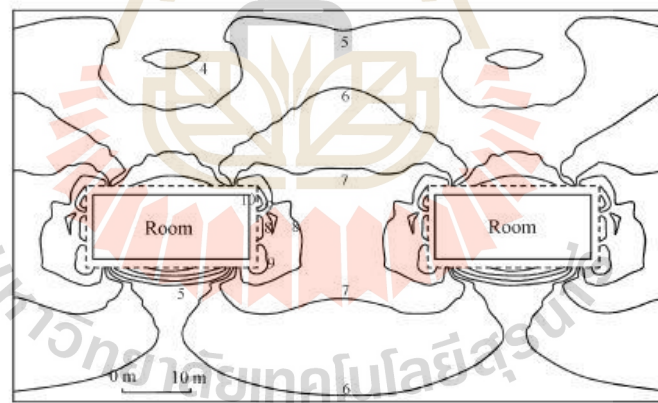
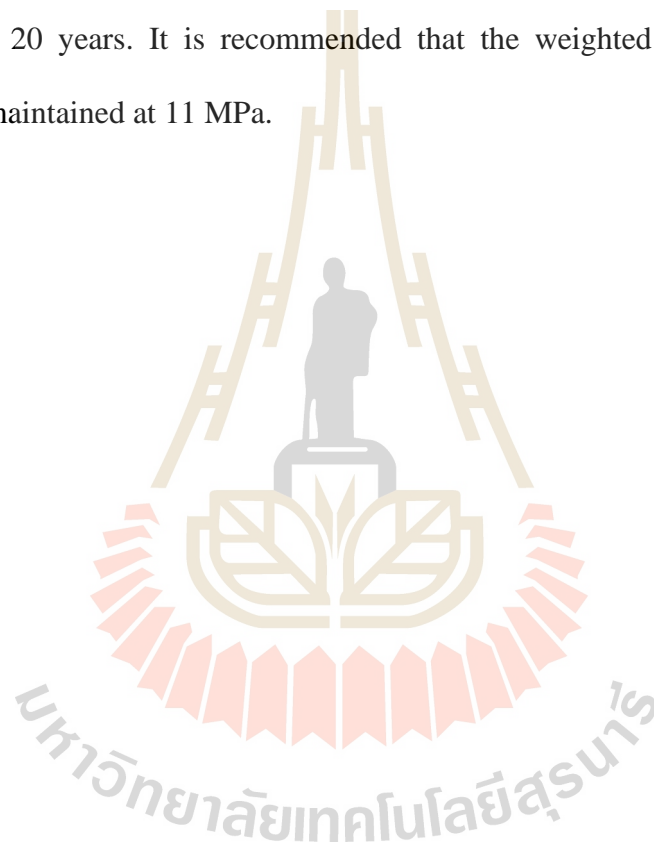


Figure 2.2 Maximum principal stress distribution around central two rooms.

Wang et al. (2015) Simulate the factors affecting the allowable width for pillars between two adjacent caverns by FLAC^{3D}. The Mohr–Coulomb criterion used to predict whether rock masses will failure. As pillar width decreases, the vertical stress distribution of the pillars changes from saddle-like to echelon-like, increase

with depth but decrease with increasing gas pressure, pillar width, and operating time. The allowable width of pillars between two adjacent bedded salt caverns, should be 2.0–2.5 times to cavern diameters.

Yang et al. (2015) studied the feasibility of abandoned salt caverns for large-scale underground energy storage. The maximum volume shrinkage of the cavern is less than 25% and the maximum deformations of diameters after operating are less than 2% for 20 years. It is recommended that the weighted average internal gas pressure be maintained at 11 MPa.



CHAPTER III

LABORATORY TESTS

3.1 Introduction

This chapter describes the rock salt sample preparation, apparatus and test methods to experimentally determine the time-dependent deformations of rock salt under triaxial cyclic loading so as to determine mechanical stability of salt under different storage conditions.

3.2 Sample preparation

The salt specimens tested here are obtained from ASEAN Potash Chaiyaphum Public Company Limited, Chaiyaphum province. Salt blocks are collected from Lower Members of Maha Sarakham formation. This salt member has long been considered as a host rock for compressed-air energy storage by the Thai Department of Energy. Sample preparation is conducted in laboratory facility at the Suranaree University of Technology. The salt blocks are dry-cut and ground as shown in Figure 3.1. The salt specimens are prepared as rectangular blocks with nominal dimensions of 54×54×108 mm³, as shown in Figure 3.2. The specimens are relatively pure halite with slight amount (less than 1-2 %) of anhydrite, clay minerals and ferrous oxide. Warren (1999) gives detailed descriptions of the salt origin and geology of Maha Sarakham formation. A total of 12 specimens are prepared for testing. Table 3.1 summarizes the specimen number, dimensions and density.



Figure 3.1 Salt specimen is dry-cut by cutting device.

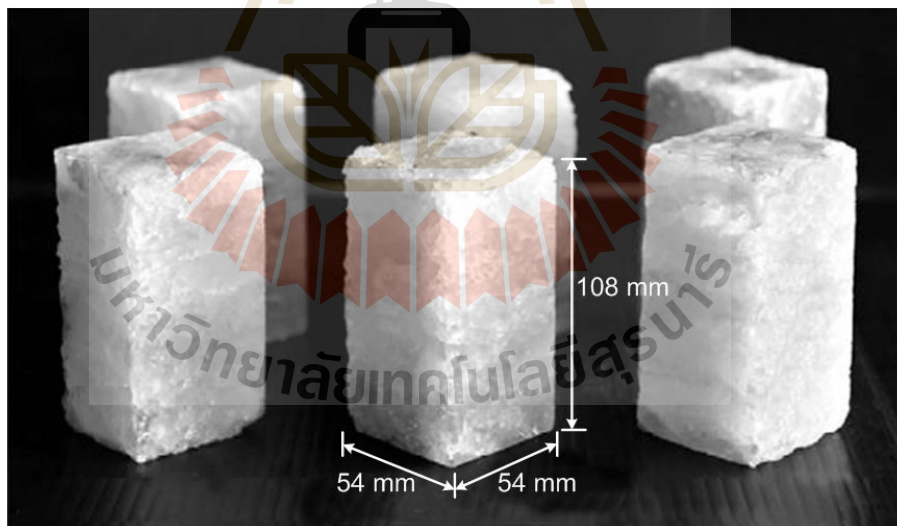


Figure 3.2 Some rectangular specimens of salt used in triaxial static and cyclic loading testing.

Table 3.1 Salt specimens prepared for triaxial cyclic loading tests.

Specimen No.	Width (mm)	Length (mm)	Height (mm)	Weight (g)
LS-TCL-01	53.6	54.5	108.9	557.5
LS-TCL-02	54.4	55.3	109.1	578.2
LS-TCL-03	52.9	54.1	108.1	544.0
LS-TCL-04	53.9	53.7	107.3	547.0
LS-TCL-05	53.7	54.9	109.8	556.2
LS-TCL-06	51.7	54.6	108.5	560.5
LS-TCL-07	53.8	54.6	108.4	553.5
LS-TCL-08	53.8	54.5	107.2	550.5
LS-TCL-09	55.3	54.5	107.1	545.0
LS-TCL-10	54.1	54.3	108.1	545.8
LS-TCL-11	54.3	54.7	107.9	547.1
LS-TCL -12	54.6	54.8	107.5	545.3

3.3 Test apparatus and method

Triaxial cyclic loading test is performed to predict the time-dependent deformation of salt under static and cyclic loadings. A polyaxial load frame (Fuenkajorn et al., 2012) is used to apply axial and lateral stresses to the rectangular salt specimens (Figure 3.3). The test frame utilizes two pairs of cantilever beams to apply lateral stresses. The axial stress is applied by a hydraulic cylinder connected to an electric pump. The frame has an advantage over the conventional triaxial Hoek cell because it

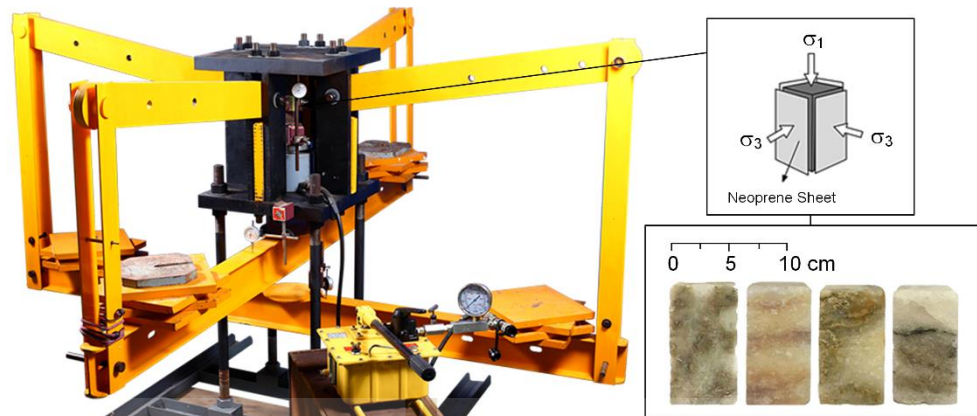


Figure 3.3 Polyaxial load frame used in triaxial cyclic loading testing (Fuenkajorn et al., 2012).

allows a relatively quick installation of the test specimen under triaxial condition while the lateral expansion and contraction can be measured.

To simulate the stress conditions under storage operation, the tributary area concept (Obert and Duvall, 1967) is used (Figure 3.4). The axial stress (σ_1) is applied on the specimens for the equivalent extraction ratios (e) of 30, 40 and 60%. The maximum and minimum lateral stresses (σ_3) used during cyclic loading are defined as 90% and 20% of the in-situ stresses (at the mine roof simulated at the depths of 250, 300, 350 and 400 m.

The test method can be separated into two series :

1. Static loading test (after mine excavation but before storage operation)
2. Cyclic loading test (pressure injection and withdrawal during storage operation)

For static loading test, the tributary area concept is applied to determine the equivalent pillar stress (σ_P) for the extraction ratios of 30%, 40% and 60. According to Hedley (1967), the strain is not constant as the pillar height changes. This causes the

convergence to change proportionally to the pillar height. It is assumed that the pillar height does not affect the extraction ratio because the extraction ratio is only dependent on the area. The extraction ratio is a function of the pillar width and the room width, and it is defined by the following:

$$\text{Extraction ratios (e)} = [((W_p+W_o)^2 - W_p^2)/(W_p+W_o)^2] \quad (3.1)$$

where W_p is the pillar width of a square pillar and W_o is the room width.

The pillar stress in terms of the extraction ratio (e) can be written as (Hoek and Brown, 1980):

$$\sigma_v = \rho \cdot H \quad (3.2)$$

$$\sigma_p = [(\rho \cdot H)/(100 - e)] \times 100 \quad (3.3)$$

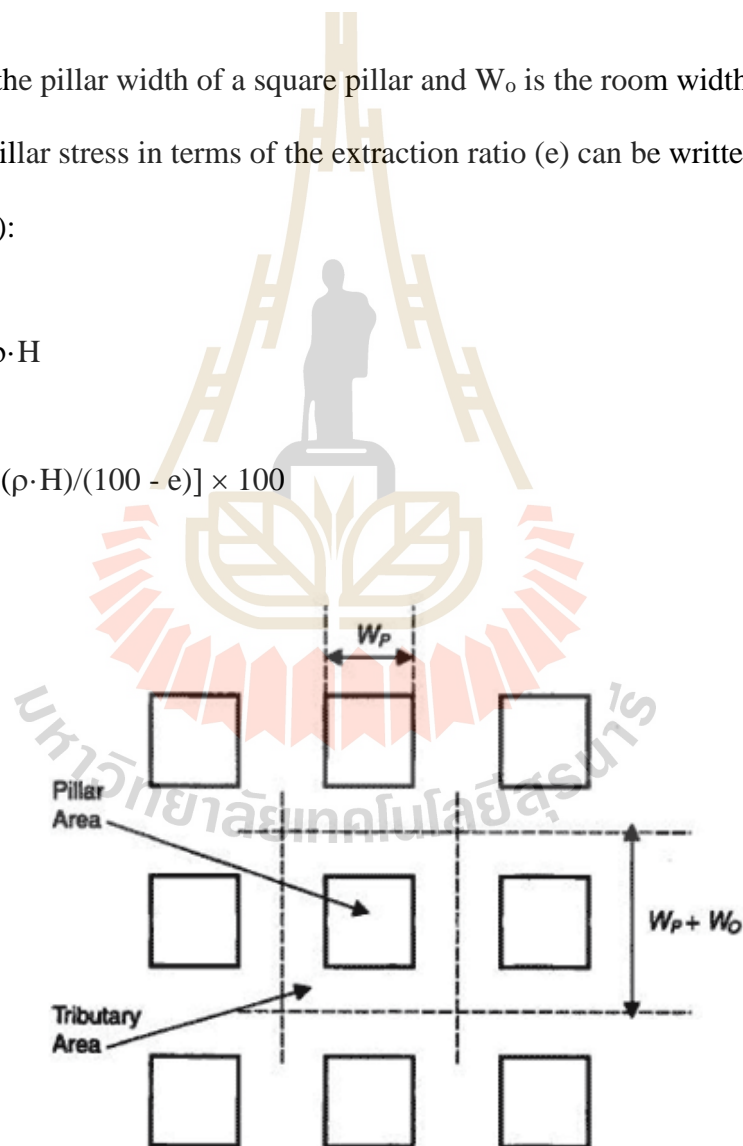


Figure 3.4 Tributary area concept. (Farmer and Gilbert, 1984).

where σ_v is vertical in-situ stress, H is the mine depth, and ρ is in-situ stress gradient of overburden (approximated here as 0.021 MPa/m). The calculations are made for the depths of 250, 300, 350 and 400 m. The static loading test is performed to simulate the salt pillars (after excavation). After installing the salt specimen into the polyaxial load frame, dead weights are placed on the cantilever beams at the bottom connected to a steel rod on the other end of the fixed beam. Neoprene sheets are placed at the interface between loading platens and rock surfaces to minimize friction. A constant axial stresses (σ_1 or simulated σ_p) is first applied to the rock specimens range from 7.5 to 21 MPa for the depths of 250, 300, 350 and 400 m. For each depth, extraction ratios are varied from 30, 40 to 60%. The specimen deformations are monitored by four displacement dial gages with high precision (± 0.01 mm) placing vertically and horizontally on the opposite sides of the specimen. The readings are recorded every 30 seconds, immediately after applying the axial load. The reading intervals are gradually increased to every half hour after 3 hours of testing. The static test period is 5 days, as shown in Figure 3.5. Table 3.2 shows the loading conditions for static loading test. The mean stress (σ_m) and octahedral shear stress (τ_{oct}) equivalent to the σ_p are also calculated (Jaeger et al., 2007):

$$\sigma_m = (\sigma_p/3) \quad (3.4)$$

$$\tau_{oct} = \frac{\sqrt{2}}{3}(\sigma_p) \quad (3.5)$$

where σ_p is equivalent pillar stress depending on the extraction ratio.

Table 3.2 Loading conditions for static loading test

Depth (m)	σ_v (MPa)	e (%)	σ_p (MPa)	σ_m (MPa)	τ_{oct} (MPa)
250	5.25	30	7.50	2.50	3.54
		40	8.75	2.92	4.12
		60	13.13	4.38	6.19
300	6.30	30	9.00	3.00	4.24
		40	10.50	3.50	4.95
		60	15.75	5.25	7.42
350	7.35	30	10.50	3.50	4.95
		40	12.25	4.08	5.77
		60	18.38	6.13	8.66
400	8.40	30	12.00	4.00	5.66
		40	14.00	4.67	6.60
		60	21.00	7.00	9.90

For cyclic loading test, the axial and lateral stresses in terms of the injection and withdrawal pressures (P_{max} and P_{min}) can be written as :

Loading during injection stage :

$$\sigma_1 = \sigma_p - 90\% \sigma_v \cdot e \quad (3.6)$$

$$\sigma_3 = P_{max} = 90\% \sigma_v \quad (3.7)$$

Loading during withdrawal stage :

$$\sigma_1 = \sigma_p - 20\% \sigma_v \cdot e \quad (3.8)$$

$$\sigma_3 = P_{min} = 20\% \sigma_v \quad (3.9)$$

The cyclic loading test is subsequently performed on the same specimens after the strains under static loading have been recorded for 5 days. This is to simulate compressed-air injection. The confining pressures on salt specimens are increased to the selected maximum pressure (P_{\max}) which is defined as 90% of the in-situ stresses, and the selected axial stress is decreased for each specimen. In this stage, the specimens are tested for 12 hours. For the withdrawal stage, the confining pressures on salt specimens are decreased to the selected minimum pressure (P_{\min}), defined as 20% of the in-situ stresses, and increased the axial stress accordingly. In this stage, the specimens are tested for 12 hours. The loading cycle is repeated for 21 cycles (21 days). Table 3.3 and Figure 3.4 show the loading conditions for the cyclic loading test.

Table 3.3 Loading conditions for cyclic loading test

Depth (m)	σ_v (MPa)	e (%)	σ_p (MPa)	$\sigma_{1,\text{inject}}$ (MPa)	$\sigma_{1,\text{with}}$ (MPa)	$P_{\max,\text{inject}}$ (MPa)	$P_{\min,\text{with}}$ (MPa)	$\tau_{\text{oct},\text{min}}$ (MPa)	$\tau_{\text{oct},\text{max}}$ (MPa)
250	5.25	30	7.50	6.08	7.19	4.73	1.05	0.64	2.89
		40	8.75	6.86	8.33			1.01	3.43
		60	13.13	10.29	12.50			2.62	5.40
300	6.30	30	9.00	7.30	8.62	5.67	1.26	0.77	3.47
		40	10.50	8.23	10.00			1.21	4.12
		60	15.75	12.35	14.99			3.15	6.47
350	7.35	30	10.50	8.52	10.06	6.62	1.47	0.90	4.05
		40	12.25	9.60	11.66			1.41	4.80
		60	18.38	14.41	17.49			3.67	7.55
400	8.40	30	12.00	9.73	11.50	7.56	1.68	1.02	4.63
		40	14.00	10.98	13.33			1.61	5.49
		60	21.00	16.46	19.99			4.20	8.63

Note : σ_m is mean stress = $(\sigma_1 + 2\sigma_3)/3$

P_{max} or $\sigma_{3,inject}$ is maximum pressure (during injection) = $90\% \cdot \sigma_v$

P_{min} or $\sigma_{3,with}$ is minimum pressure (during withdrawal) = $20\% \cdot \sigma_v$

$\tau_{oct,max}$ is octahedral shear stress under withdrawal condition

$$\tau_{oct,max} = \frac{\sqrt{2}}{3} (\sigma_{1with} - \sigma_{3with})$$

$\tau_{oct,min}$ is octahedral shear stress under injection condition

$$\tau_{oct,min} = \frac{\sqrt{2}}{3} (\sigma_{1inject} - \sigma_{3inject})$$

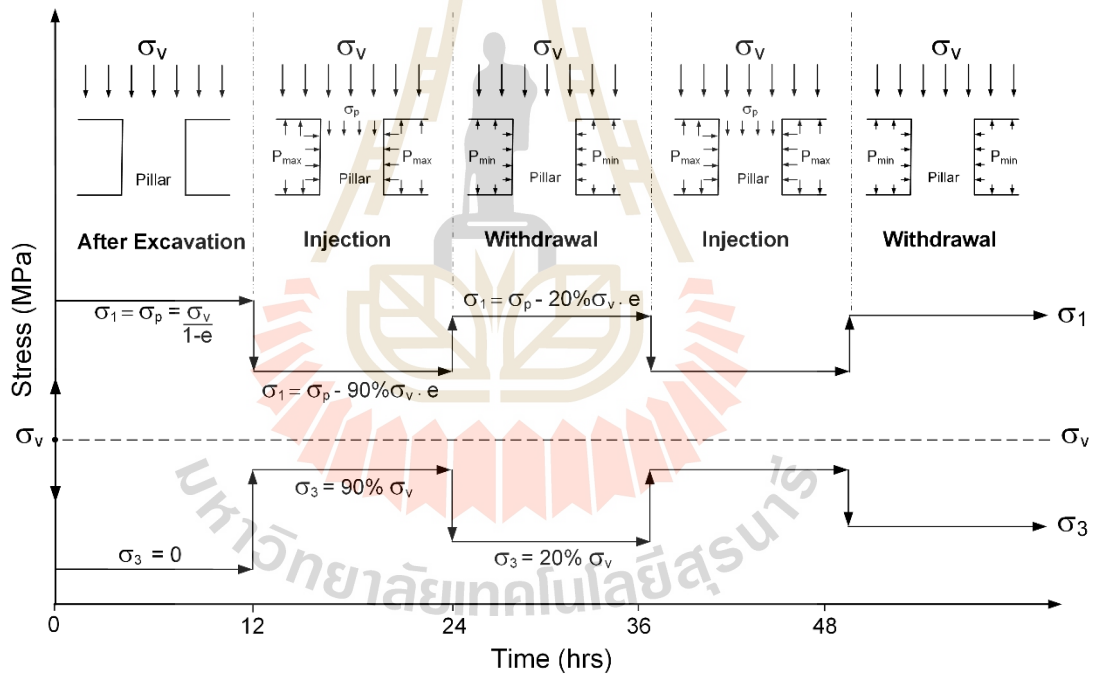


Figure 3.5 Cyclic loading paths as function of time.

CHAPTER IV

TEST RESULTS

4.1 Introduction

This chapter describes the laboratory results of the triaxial static and cyclic loading tests. Comparisons of the strains results obtained under different test parameters (extraction ratio, depth, etc.) are made. Discussions on the reliability of the measurement results are given. The test results will be used to calibrate the creep parameters for predicting long-term behavior of salt.

4.2 Static loading test results

For the static loading, the constant axial stresses range from 7.1 to 20.0 MPa. The vertical and lateral displacements are monitored. The test results are presented in the form of the axial and lateral strain-time curves. The axial and lateral strain-time curves for the static loading with constant axial stress are determined. Figures 4.1 through 4.4 show the test results. Each salt specimen shows instantaneous, transient, and steady-state creep phases. The salt specimens continue to deform without failure. The creep deformation increases with increasing axial stresses. The static test results generally agree with those of Fuenkajorn and Phueakphum (2010), Archeeploha and Fuenkajorn (2013) and Wilalak and Fuenkajorn (2016) who perform uniaxial creep testing on the same Maha Sarakham salt. For each depth (each vertical in-situ stress), the instantaneous and creep strains increase with pillar stress (σ_p) and extraction ratio (e).

The strain rate, in visco-plastic (steady-state) phase in particular, increases with increasing opening depth. The largest strain rate is observed for the opening depth of 400 m ($\sigma_v = 8.4$ MPa) and under highest extraction ratio of 60%, as shown in Figure 4.4. The lowest strain rate is obtained for the specimens that are simulated at shallowest depth (200 m) and under lowest extraction ratio of 30% (Figure 4.1)

4.3 Cyclic loading test results

The cyclic loading is performed immediately after the static loading reached 5 days. Figures 4.5 through 4.8 show the results for the simulated depths of 250, 300, 350 and 400 m. The maximum and minimum axial stresses and lateral stresses (confining pressures) that have been pre-calculated (as shown in Table 3.3), are cyclically applied to the salt specimens till the end of testing (21 days). These stresses are calculated under three different extraction ratios: $e = 30, 40$ and 60%.

The axial and lateral strains vs. time curves are plotted in the diagrams in Figures 4.5 through 4.8. From these curves, it can be clearly seen that the visco-plastic strains show up-down values corresponding to the maximum and minimum octahedral shear stresses applied during retrieval and injection periods. The strain fluctuation is observed on both axial and lateral directions. Under injection, the axial strains decrease while the lateral strains increase. For each cycle, small instantaneous and visco-elastic creep strains have been detected during under both injection and withdrawal periods. The differences between the maximum and minimum strains tend to remain relatively-constant through the testing period. For all depths, the largest strain differences occur under higher extraction ratio ($e = 60\%$). The average trend of the visco-plastic strains increases with time (or with loading cycles). The increasing

rates are higher for larger extraction ratio. This holds true for all depths. The differences of the maximum and minimum strains and the increasing rates of the overall plastic strain also increase with opening depths (compared Figure 4.5 and Figure 4.8). The measured strains during cyclic loading seem reliable, as evidenced by comparing the results obtained under different test parameters. For example, in Figure 4.5, the fluctuation of the axial and lateral strains appears to be consistent throughout the test period. The loci of the maximum axial strains, in particular, show the strain rate that coincides with those of the static loading for each extraction ratio. This observation is also found for the depths of 300, 400 and 500 m, as shown in Figures 4.6 through 4.9. This suggests that the salt pillars under storage conditions within the range of the test parameters used here would show similar vertical creep deformation to those of the static loading condition, i.e. under mine excavation operation. Some discrepancy remains on the test result, particularly for the depth of 300 m, as shown in Figure 4.6. This particular specimen tends to show inconsistent results in terms of the strains fluctuation during cyclic loading. This may be due to the intrinsic variability of the salt specimens. Their overall trends of the loci of maximum strains during cyclic loading, however, tend to agree reasonably with other specimens tested under different axial stresses (different depths).

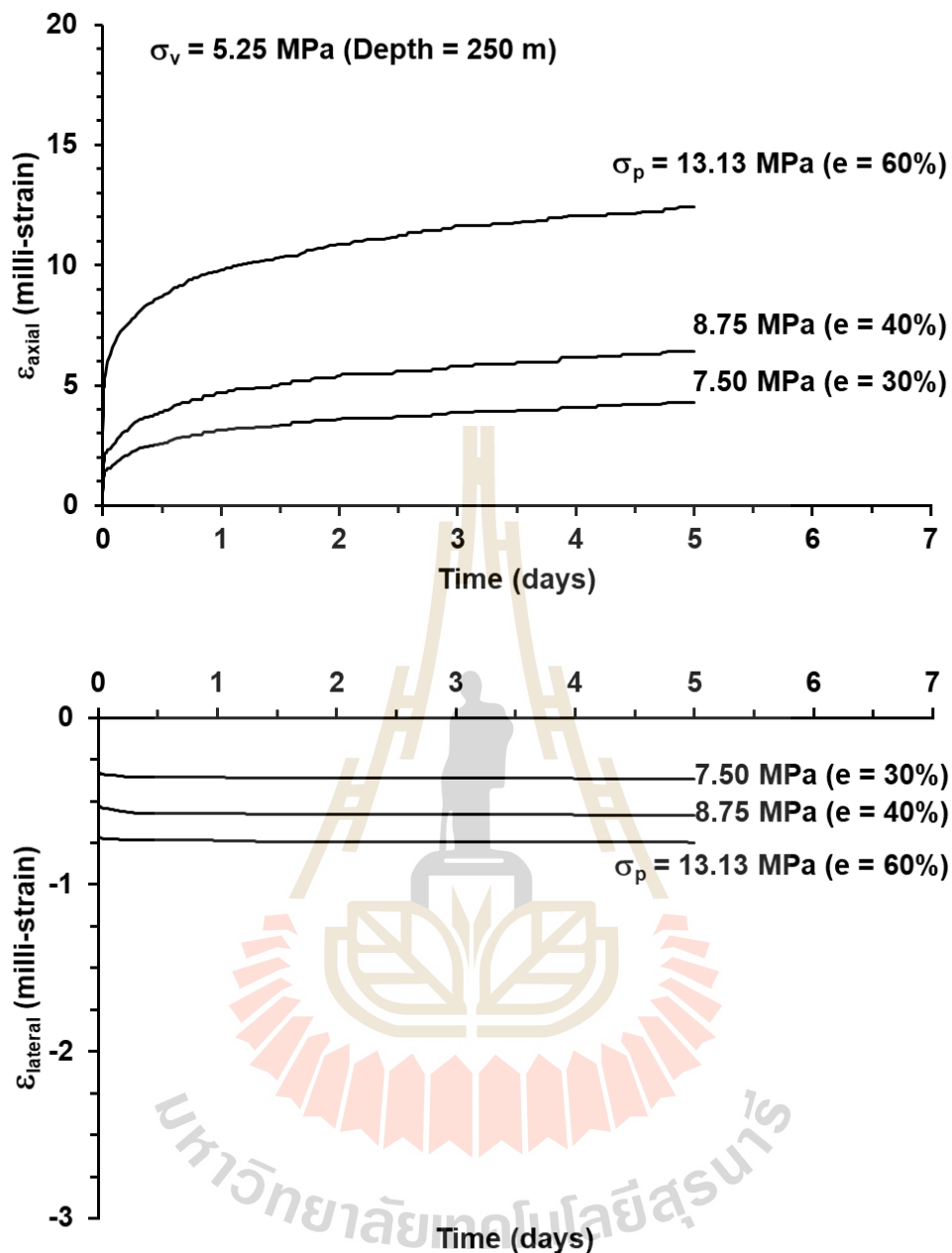


Figure 4.1 Axial and lateral strains (ϵ_{axial} , ϵ_{lat}) as a function of time (t) for static loading under maximum axial stresses (σ_p or σ_1) of 7.50, 8.75 and 13.13 MPa (for $e = 30, 40$ and 60%) at vertical stresses of 5.25 MPa or equivalent depth of 250 m.

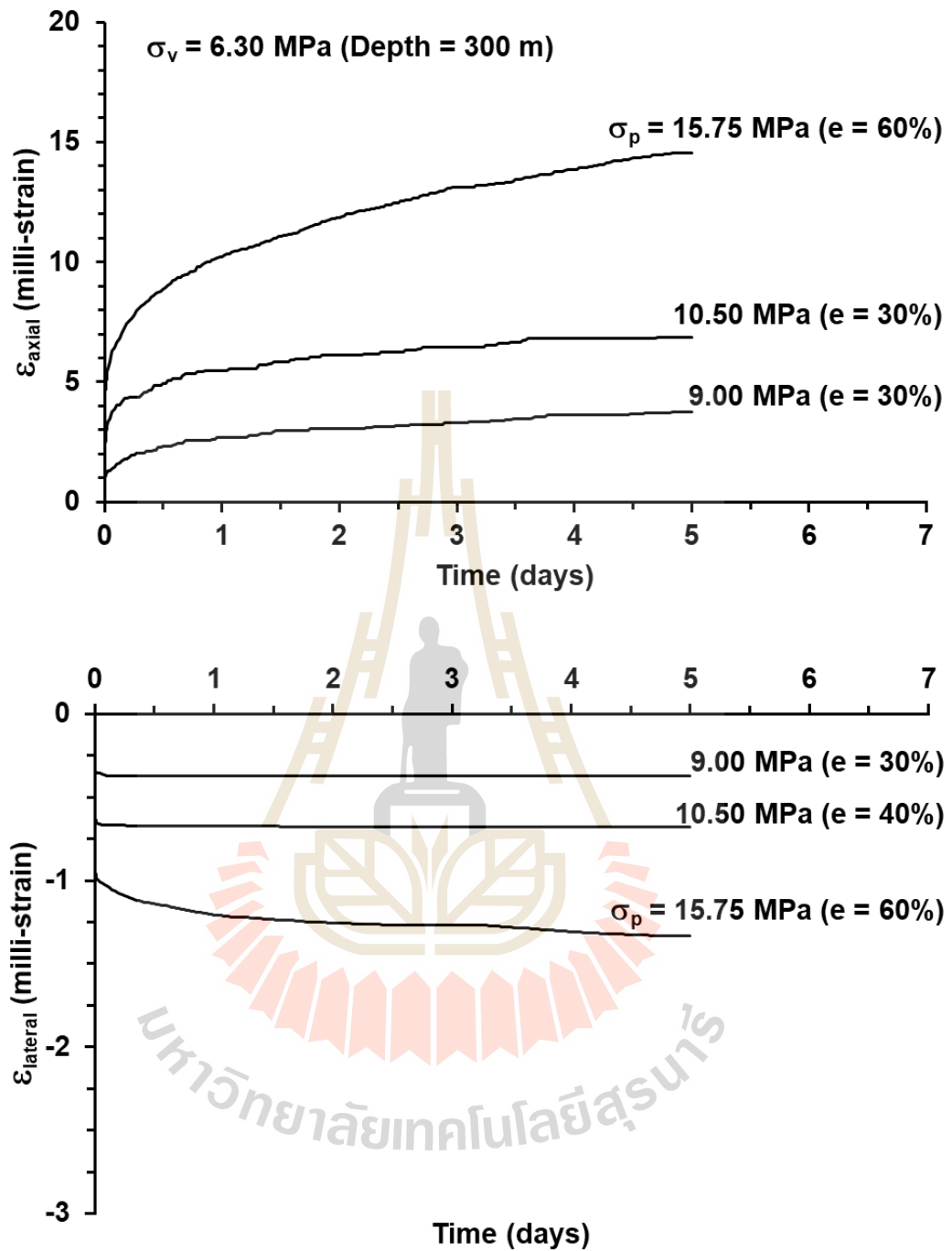


Figure 4.2 Axial and lateral strains (ϵ_{axial} , ϵ_{lat}) as a function of time (t) for static loading under maximum axial stresses (σ_p or σ_1) of 9.00, 10.50 and 15.75 MPa (for $e = 30, 40$ and 60%) at vertical stresses of 6.30 MPa or equivalent depth of 300 m.

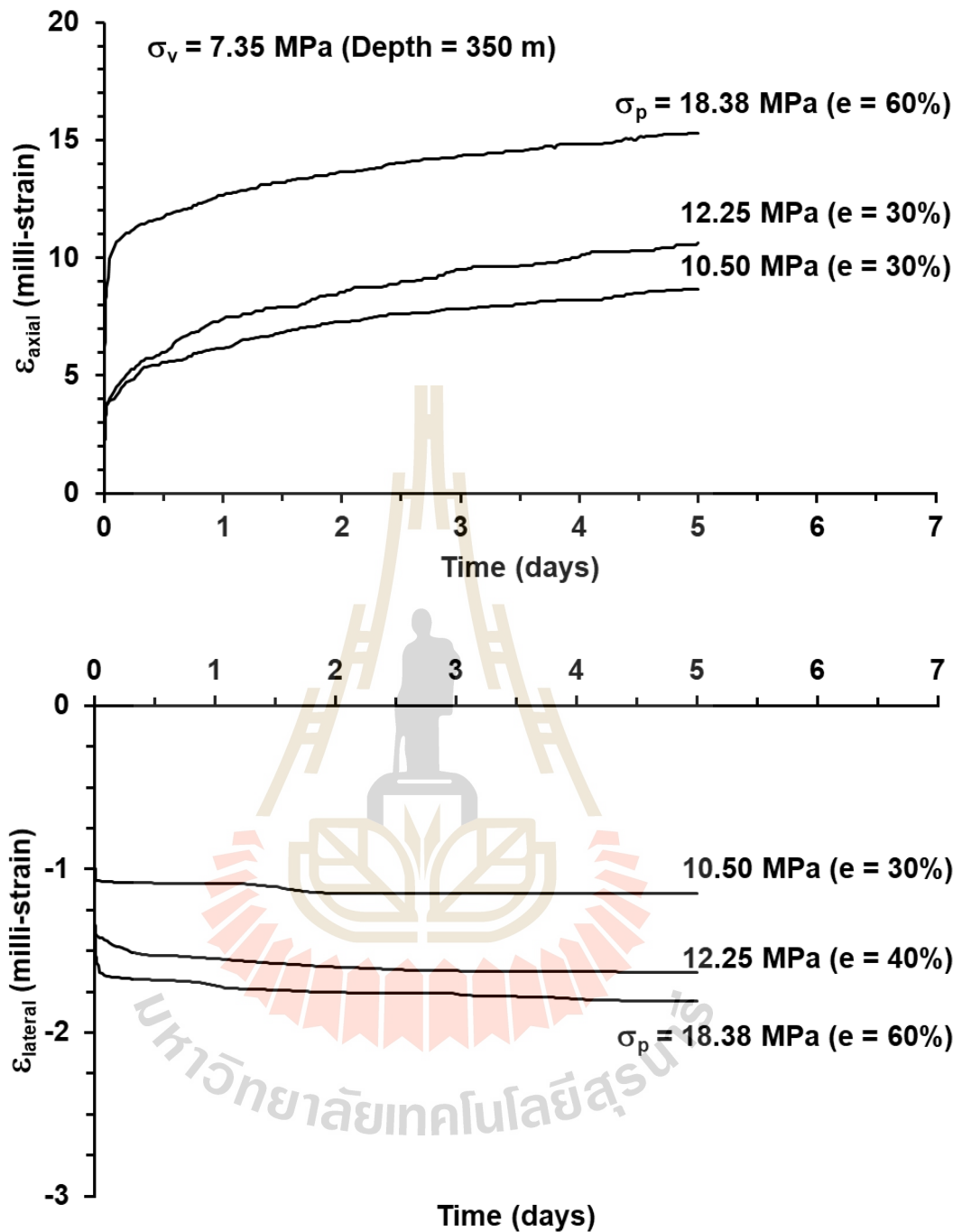


Figure 4.3 Axial and lateral strains (ϵ_{axial} , ϵ_{lat}) as a function of time (t) for static loading under maximum axial stresses (σ_p or σ_1) of 10.50, 12.25 and 18.38 MPa (for $e = 30, 40$ and 60%) at vertical stresses of 7.35 MPa or equivalent depth of 350 m.

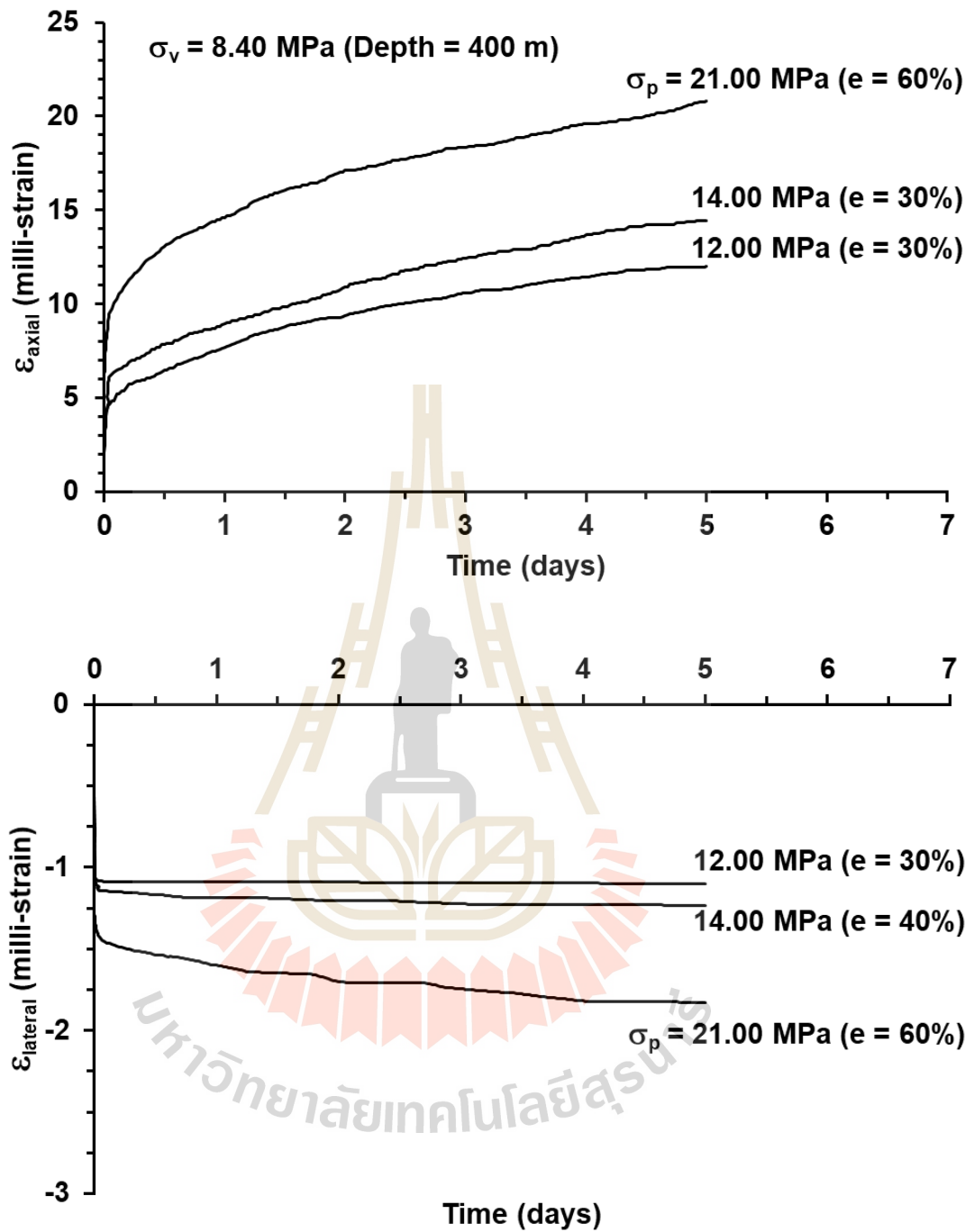


Figure 4.4 Axial and lateral strains (ϵ_{axial} , ϵ_{lat}) as a function of time (t) for static loading under maximum axial stresses (σ_p or σ_1) of 12.00, 14.00 and 21.00 MPa (for $e = 30, 40$ and 60%) at vertical stresses of 8.40 MPa or equivalent depth of 400 m.

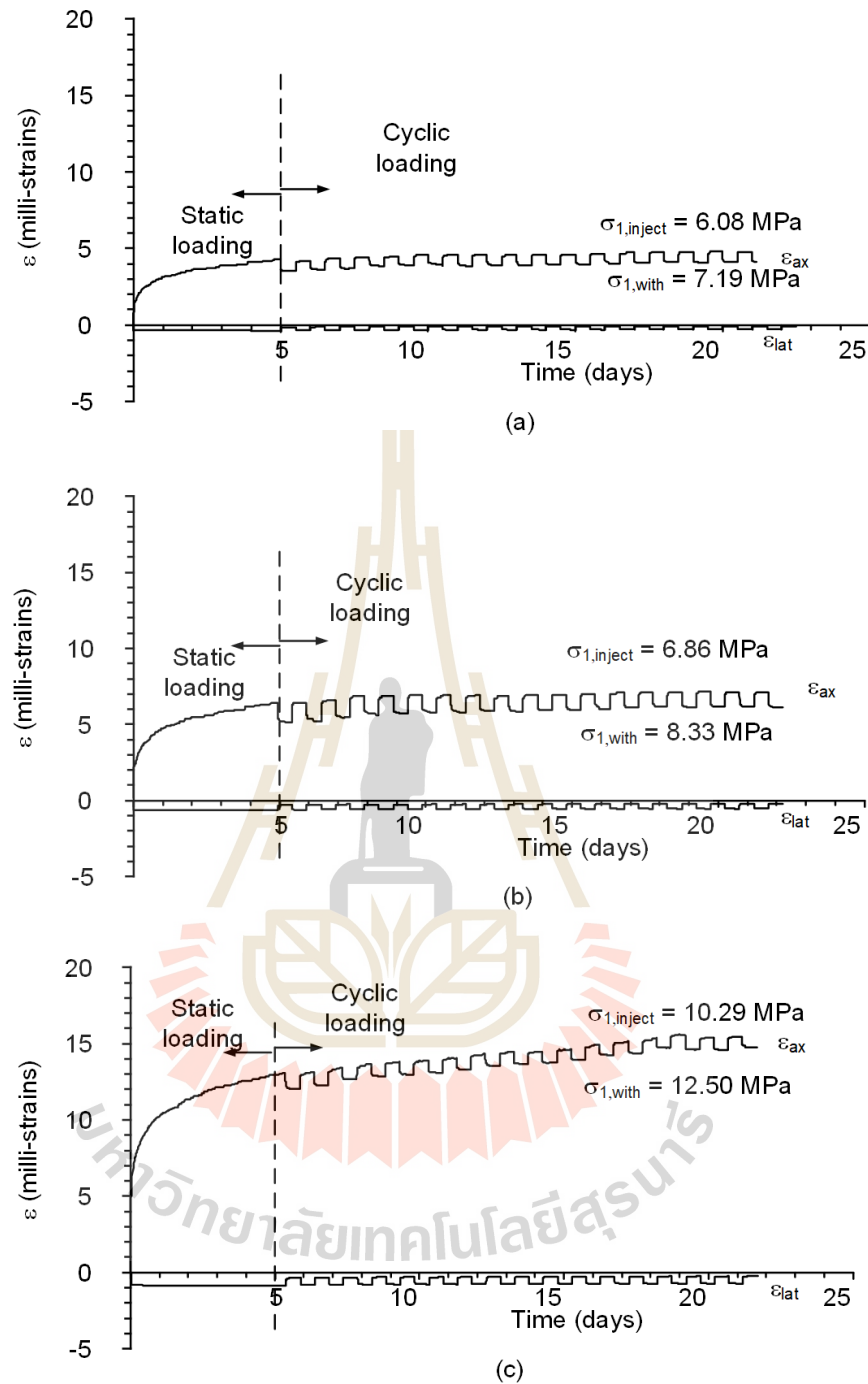


Figure 4.5 Axial (ϵ_{ax}) and lateral (ϵ_{lat}) strains as a function of time (t) simulating storage depth of 250 m ($\sigma_v = 5.25$ MPa) (a) $\sigma_{1,inject}$ and $\sigma_{1,with} = 6.08$ and 7.19 MPa ($e = 30\%$), (b) $\sigma_{1,inject}$ and $\sigma_{1,with} = 6.86$ and 8.33 MPa ($e = 40\%$) and (c) $\sigma_{1,inject}$ and $\sigma_{1,with} = 10.29$ and 12.50 MPa ($e = 60\%$).

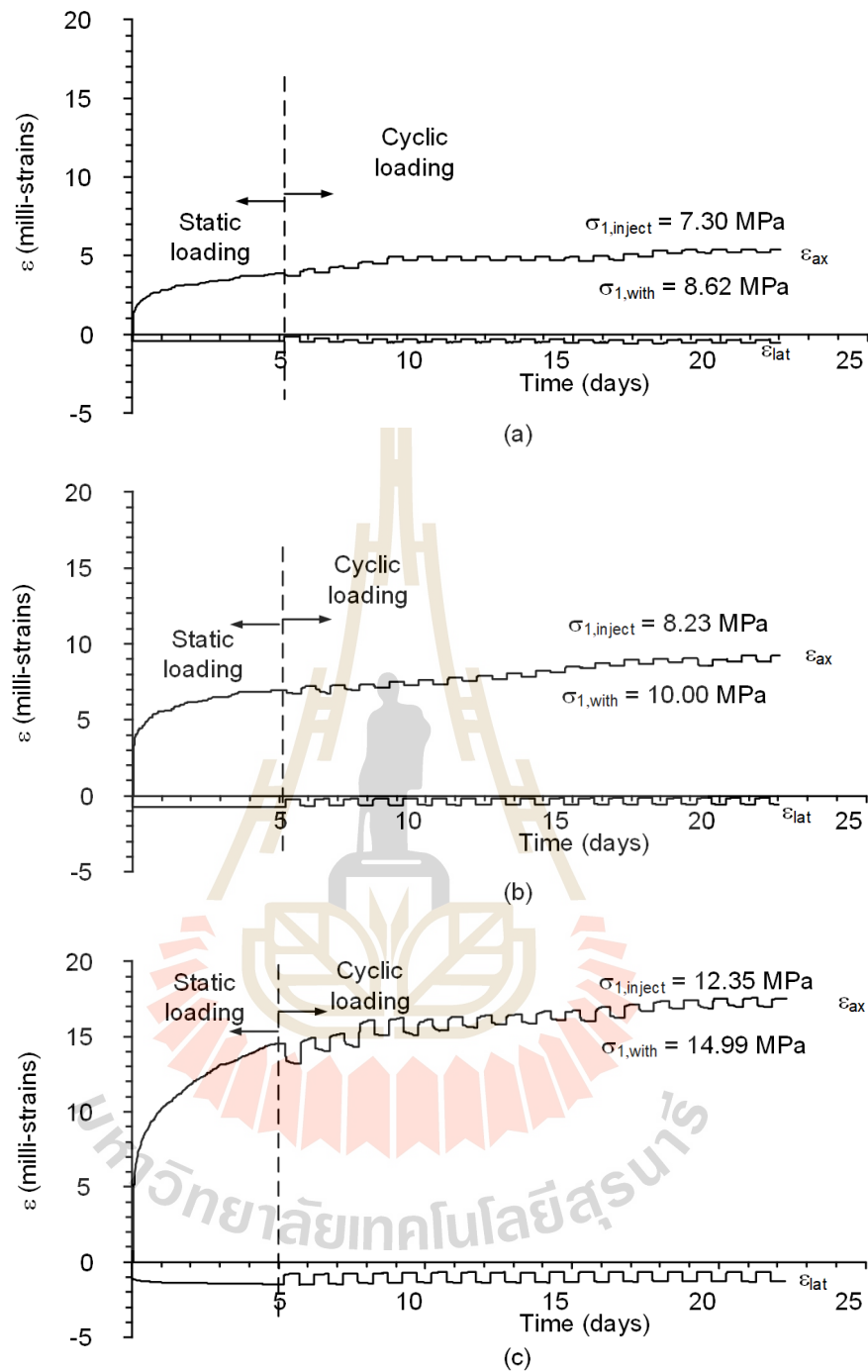


Figure 4.6 Axial (ϵ_{ax}) and lateral (ϵ_{lat}) strains as a function of time (t) simulating storage depth of 300 m ($\sigma_v = 6.30$ MPa). (a) $\sigma_{1,inject}$ and $\sigma_{1,with} = 7.30$ and 8.62 MPa ($e = 30\%$), (b) $\sigma_{1,inject}$ and $\sigma_{1,with} = 8.23$ and 10.00 MPa ($e = 40\%$) and (c) $\sigma_{1,inject}$ and $\sigma_{1,with} = 12.35$ and 14.99 MPa ($e = 60\%$).

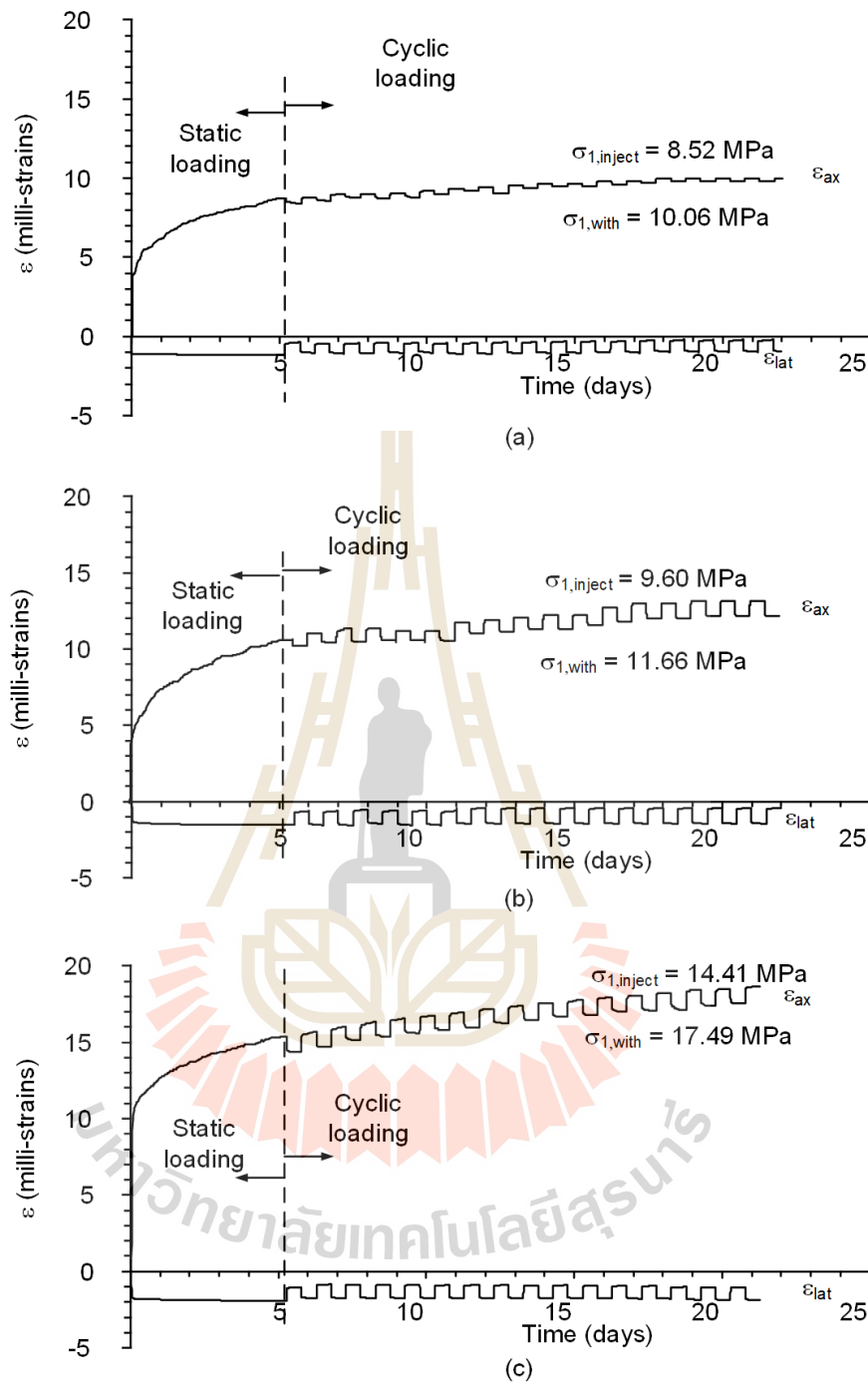


Figure 4.7 Axial (ε_{ax}) and lateral (ε_{lat}) strains as a function of time (t) simulating storage depth of 350 m ($\sigma_v = 7.35$ MPa). (a) $\sigma_{1,inject}$ and $\sigma_{1,with} = 8.52$ and 10.06 MPa ($e = 30\%$), (b) $\sigma_{1,inject}$ and $\sigma_{1,with} = 9.60$ and 11.66 MPa ($e = 40\%$) and (c) $\sigma_{1,inject}$ and $\sigma_{1,with} = 14.41$ and 17.49 MPa ($e = 60\%$).

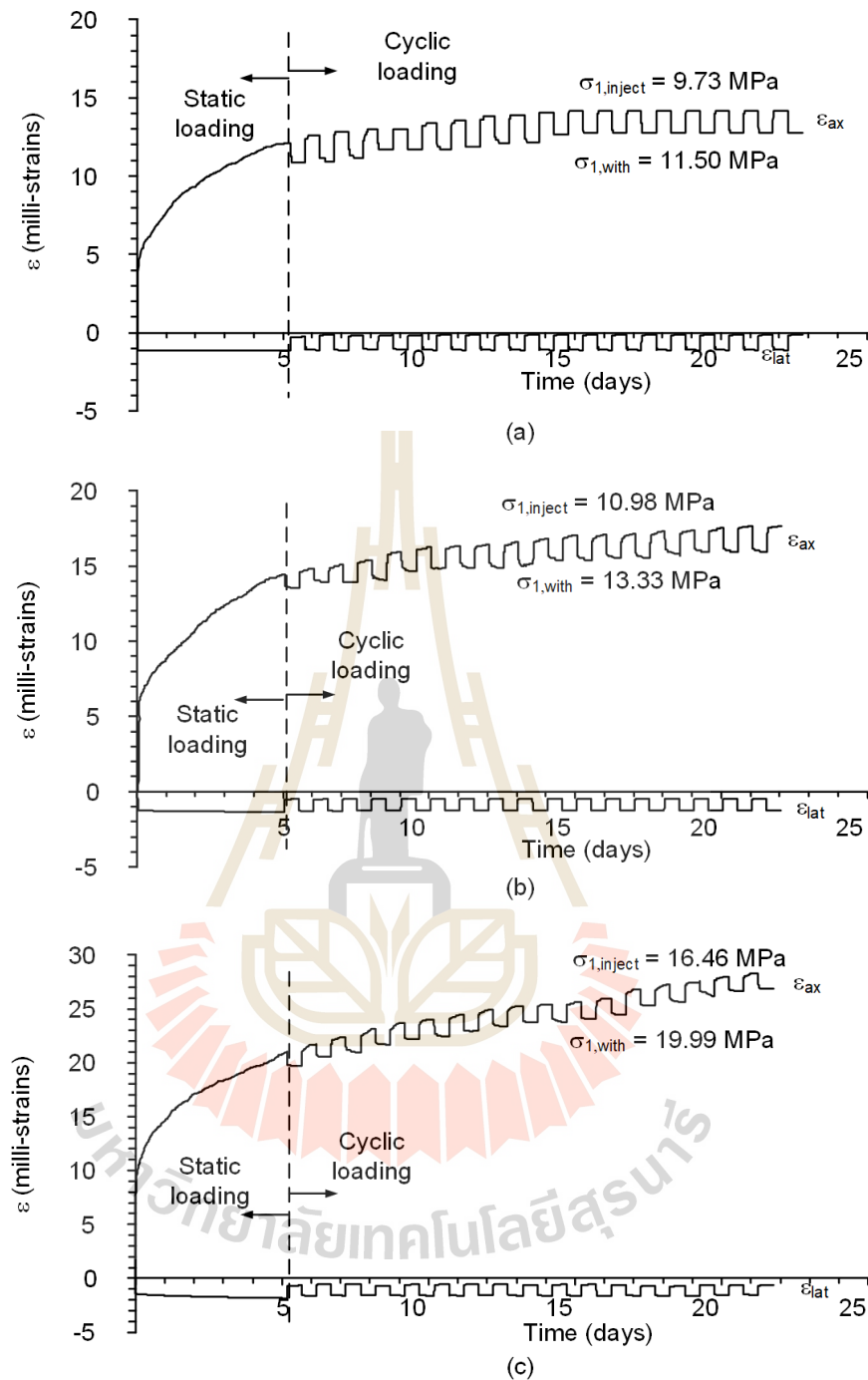


Figure 4.8 Axial (ε_{ax}) and lateral (ε_{lat}) strains as a function of time (t) simulating storage depth of 400 m ($\sigma_v = 8.40$ MPa). (a) $\sigma_{1,\text{inject}}$ and $\sigma_{1,\text{with}} = 9.73$ and 11.50 MPa ($e = 30\%$), (b) $\sigma_{1,\text{inject}}$ and $\sigma_{1,\text{with}} = 10.98$ and 13.33 MPa ($e = 40\%$) and (c) $\sigma_{1,\text{inject}}$ and $\sigma_{1,\text{with}} = 16.46$ and 19.99 MPa ($e = 60\%$).

CHAPTER V

ANALYSIS OF TEST RESULTS

5.1 Introduction

This chapter describes the calibration of creep model parameters from the cyclic loading test results. Two creep models are used: the Burgers model and potential creep law. These two creep models have been widely used to describe the time-dependent deformation of the salt. Included in this chapter are the derivations of the governing equations to comply with the boundary and loading conditions used in this study and calibration of the model parameters for each specimen.

5.2 Octahedral shear strain

Presented in this section is the derivation of the octahedral shear strain from the measured axial and lateral strains of each salt specimen. This is in order to incorporate both axial and lateral creep strains into one variable, and hence makes the calibration of the creep parameters more easily. For the triaxial stress condition, the octahedral shear strain (γ_{oct}) can be calculated from the axial (ϵ_1) and lateral (ϵ_3) strains, as follows (Jaeger et al. 2007):

$$\gamma_{\text{oct}} = \frac{\sqrt{2}}{3} \cdot (\epsilon_1 - \epsilon_3) \quad (5.1)$$

Figures 5.1 through 5.4 show the calculated octahedral shear strain results as a function of elapse time (t) for the depths of 250, 300, 350 and 400 m. Each figure shows the shear strains for three extraction ratios (30, 40 and 60%).

For all depths, the higher extraction ratios used, the greater rate are obtained from the creep shear strains. Deeper openings exhibit larger instantaneous and creep strains, as compared to the shallower ones.

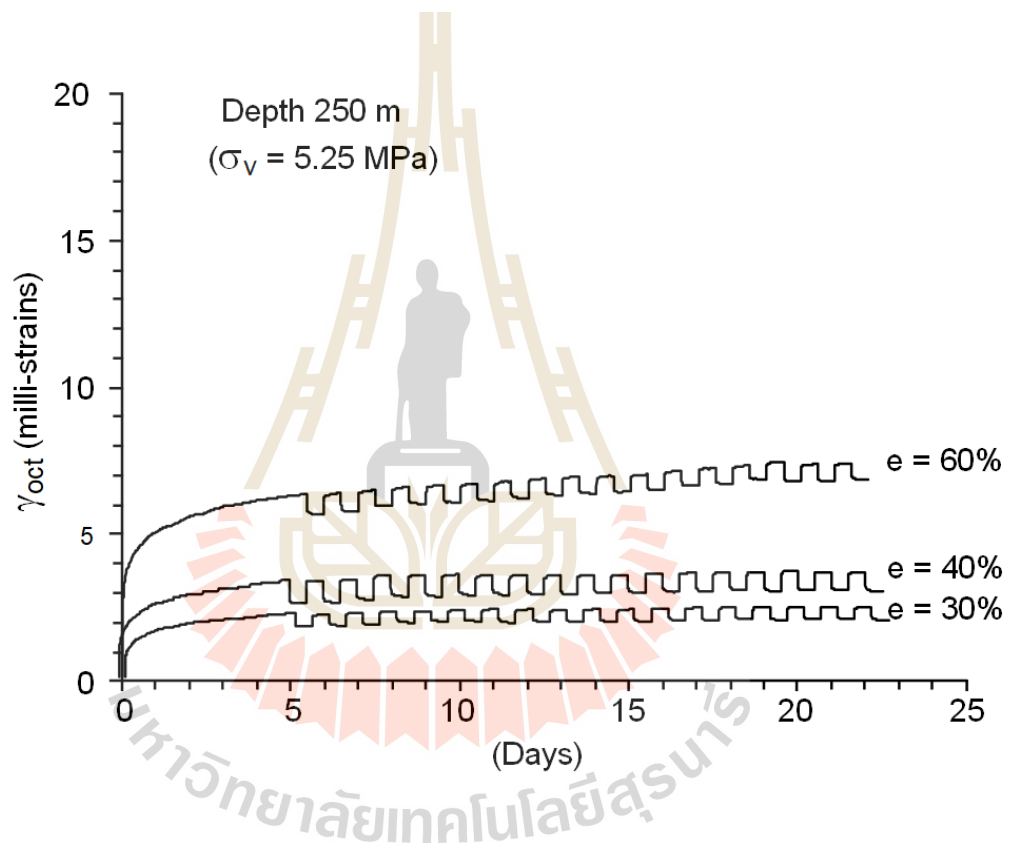


Figure 5.1 Octahedral shear strain as a function of elapse time (t) for depth of 250 m.

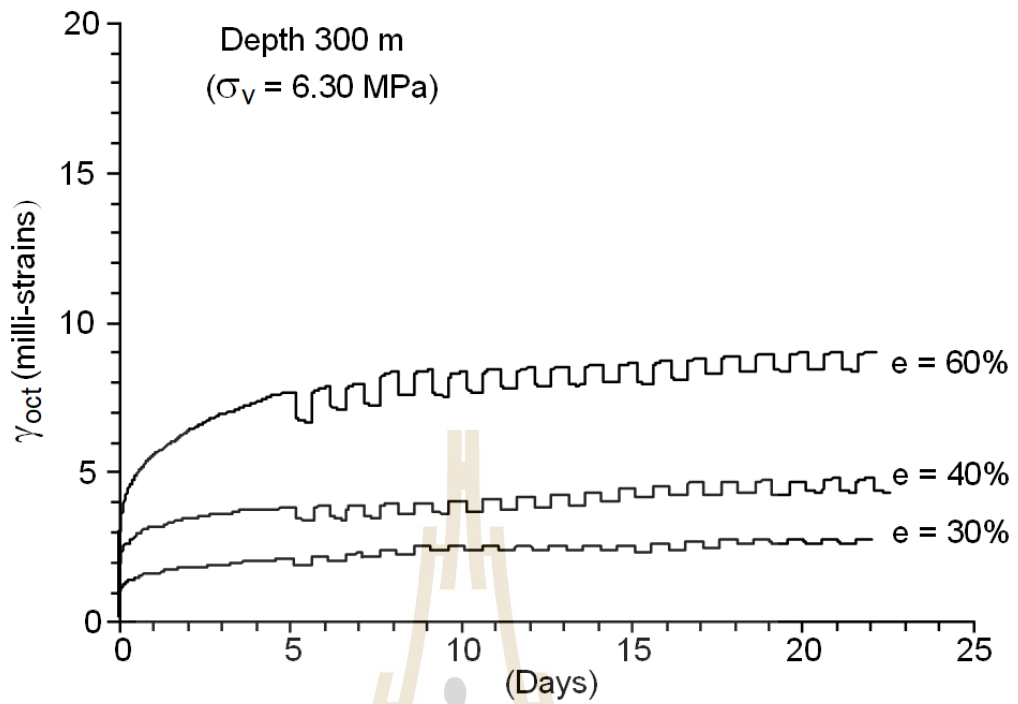


Figure 5.2 Octahedral shear strain as a function of elapse time (t) for depth of 300 m.

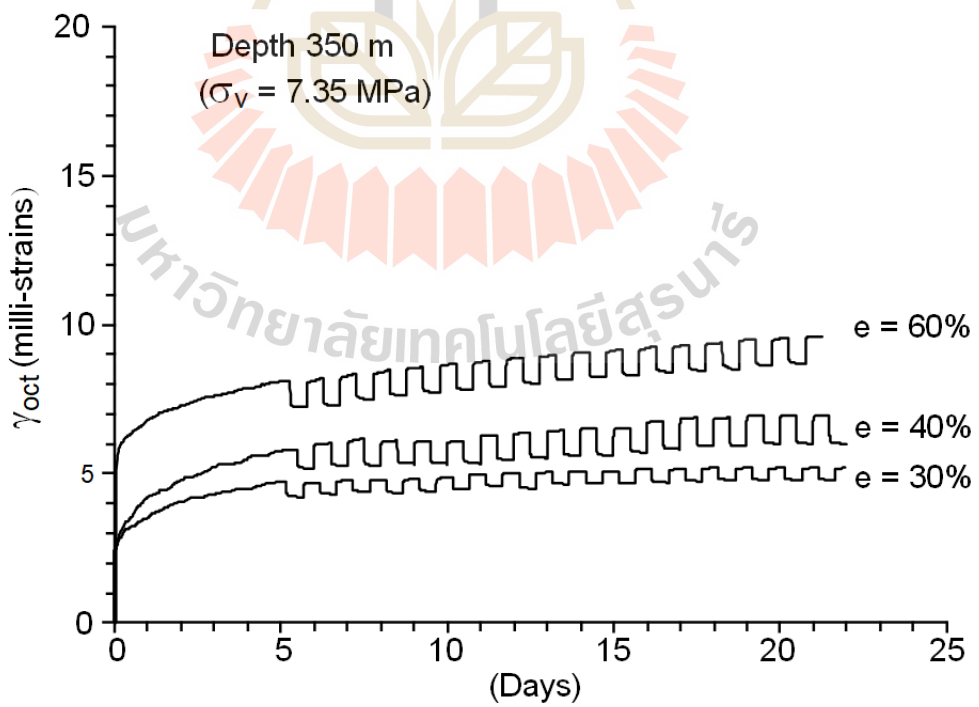


Figure 5.3 Octahedral shear strain as a function of elapse time (t) for depth of 350 m.

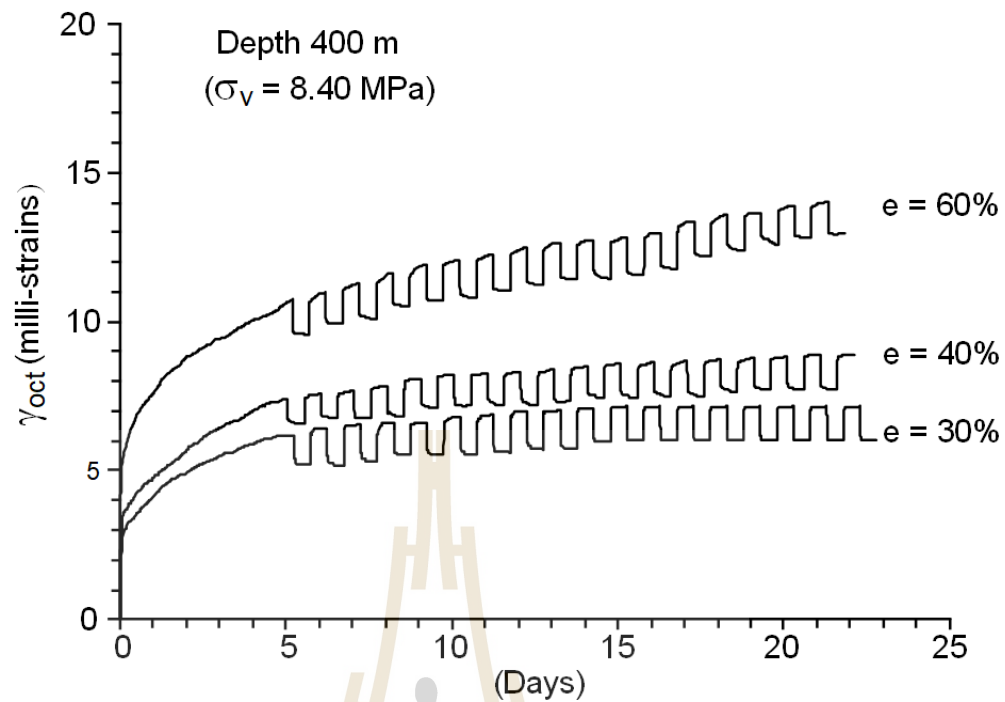


Figure 5.4 Octahedral shear strain as a function of elapse time (t) for depth of 400 m.

5.3 Calibration of creep model parameters

This section describes the derivation of creep models under triaxial stress condition and the calibration of their parameters from the test results. The calibrated model will be useful for predicting of the creep deformation and stability of salt under the durations and loading conditions beyond those used in the laboratory testing. In this study, two creep models have been used: the Burgers model and potential creep law. Both have been widely and successfully used to describe the time-dependent behavior of rock salt, particularly for the Maha Sarakham Salt (Fuenkajorn and Phueakphum, 2010; Archeeploha and Fuenkajorn, 2013; Luangthip et al., 2017; Wilalak and Fuenkajorn, 2016; and Junthong et al., 2016).

The calibration is carried out on the entire $\gamma_{\text{oct}}-t$ curves. Under cyclic loading, the maximum γ_{oct} obtained during retrieval period is used in the calibration. This will provide the conservative prediction of the pillar deformation.

5.3.1 Burgers model

The constitutive equation of the Burgers model for one-dimension problem can be written as (Findley et al., 1989):

$$\ddot{\epsilon} \left(\frac{\eta_1 \eta_2}{E_2} \right) + \dot{\epsilon} \eta_1 = \ddot{\sigma} \left(\frac{\eta_1 \eta_2}{E_1 E_2} \right) + \dot{\sigma} \left(\frac{\eta_1}{E_2} + \frac{\eta_2}{E_2} + \frac{\eta_1}{E_1} \right) + \sigma \quad (5.2)$$

where $\ddot{\epsilon}$ and $\dot{\epsilon}$ are second and first order partial derivatives of strain respect to time, $\ddot{\sigma}$ and $\dot{\sigma}$ are second and first order derivatives of stress respect to time, and σ is the applied stress. E_1 and E_2 are spring constants, and η_1 and η_2 are viscosities. Figure 5.5 shows the modular components of the Burgers model.

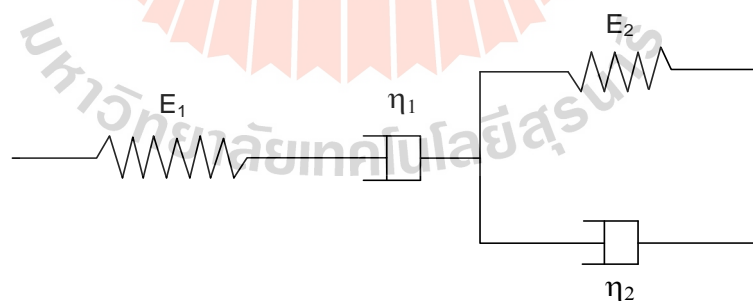


Figure 5.5 Modular components of Burgers model.

The octahedral shear strain obtained during instantaneous deformation can be calculated by (Jaeger et al., 2007):

$$\gamma_{\text{oct}} = \tau_{\text{oct}} / 2G \quad (5.3)$$

where G is the shear modulus of the salt. Via Laplace transformation, a governing equation of the Burgers model under triaxial stress state with constant applied octahedral shear stress (creep testing) can be derived (Fuenkajorn and Daemen, 1988):

$$\gamma_{\text{oct}}(t) = \tau_{\text{oct}} \left[\frac{1}{E_1} + \frac{t}{\eta_1} + \frac{1}{E_2} \left(1 - \exp\left(\frac{-E_2 t}{\eta_2} \right) \right) \right] \quad (5.4)$$

where τ_{oct} is the maximum octahedral shear stresses in MPa which is constant with time, t is the testing time in day, E_1 is the elastic modulus in GPa, E_2 is the spring constant in visco-elastic phase (GPa), η_1 is the viscosity coefficient in steady-state phase (GPa.Day), and η_2 is the viscosity coefficient in transient phase (GPa.Day).

Regression analysis with multiple variables and constants (e.g. Wendai, 2000) can determine the Burgers parameters from the test data of each specimen. Table 5.1 shows the numerical values of the Burgers parameters under different extraction ratios and depths. These parameters tend to decrease with increasing the applied octahedral shear stress. Figures 5.6 through 5.9 compare the test measurements with the predictions based on the Burgers model. The model fits well to the test results for all depths and extraction ratios. The coefficient of correlations are greater than 0.9.

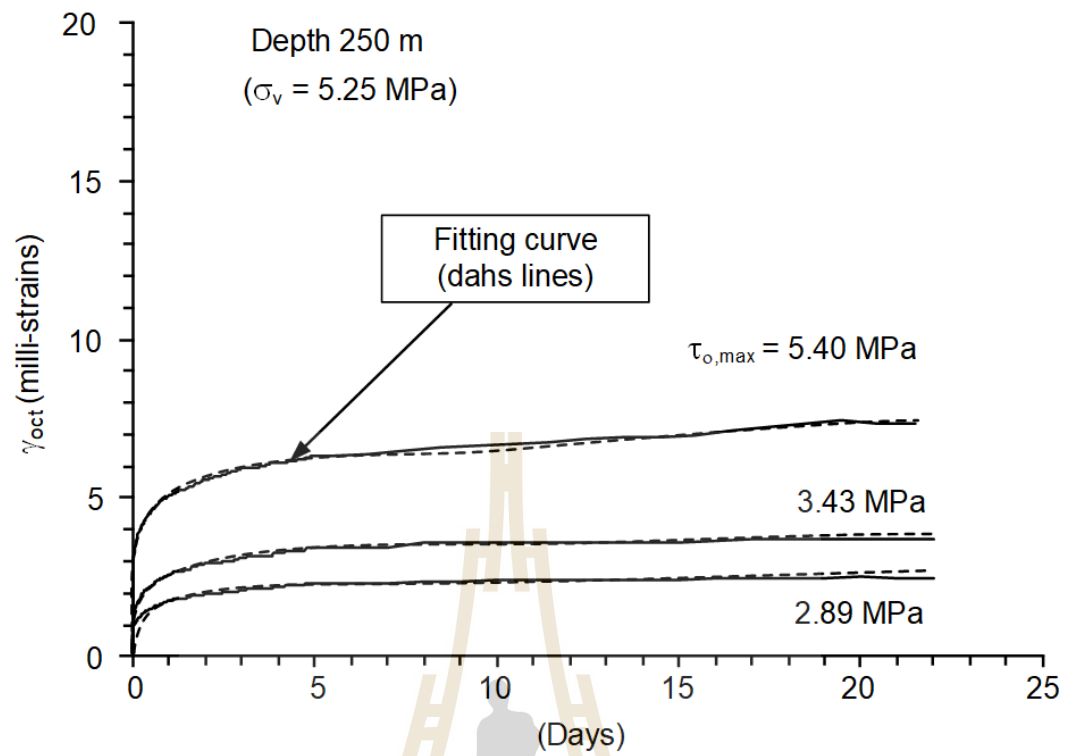


Figure 5.6 Octahedral shear strain as a function of time (solid lines) and curves fitting with Burgers model (dash lines) under octahedral shear stresses at depth 250 m.

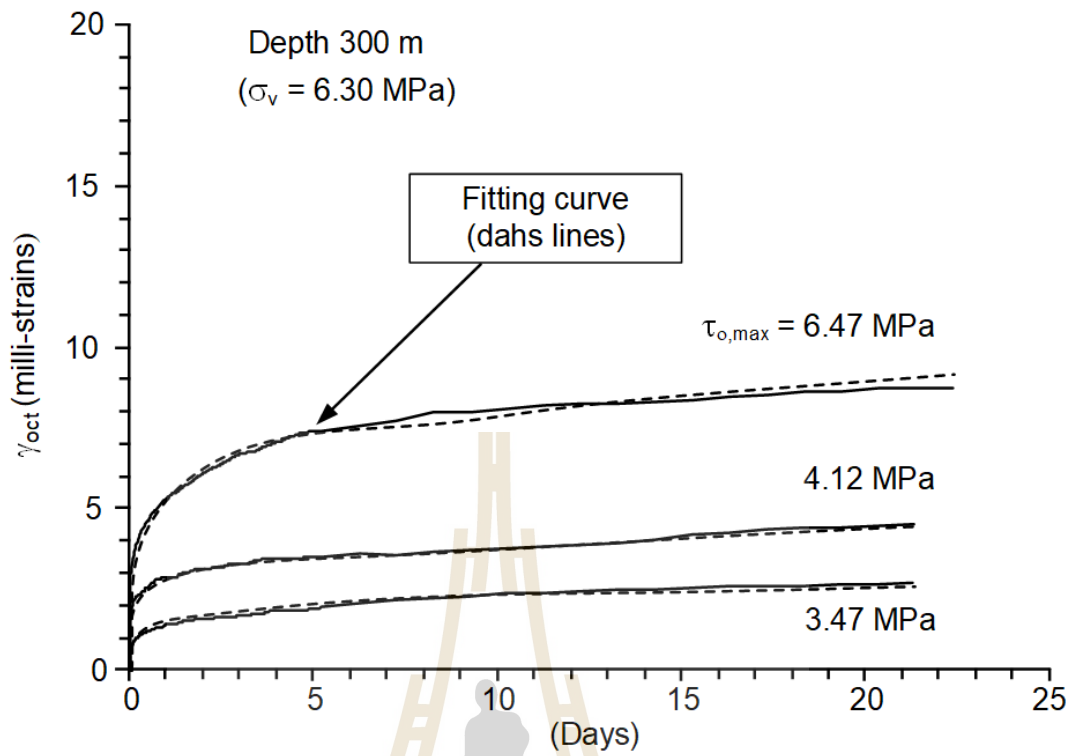


Figure 5.7 Octahedral shear strain as a function of time (solid lines) and curves fitting with Burgers model (dash lines) under octahedral shear stresses at depth 300 m.

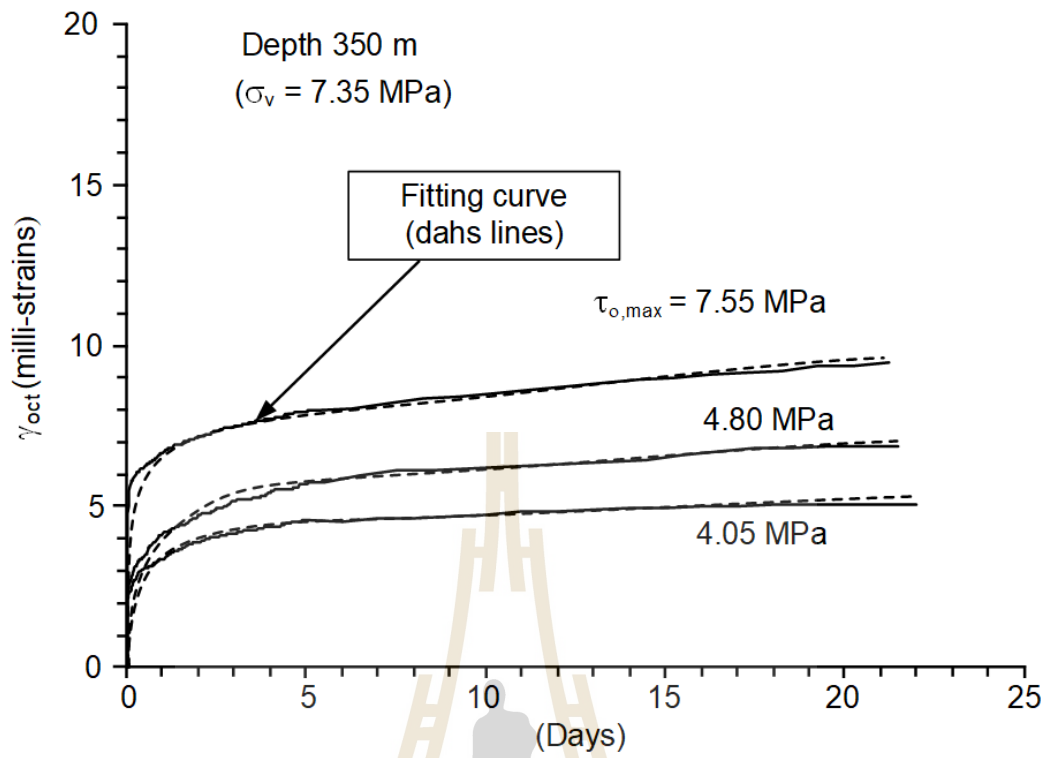


Figure 5.8 Octahedral shear strain as a function of time (solid lines) and curves fitting with Burgers model (dash lines) under octahedral shear stresses at depth 350 m.

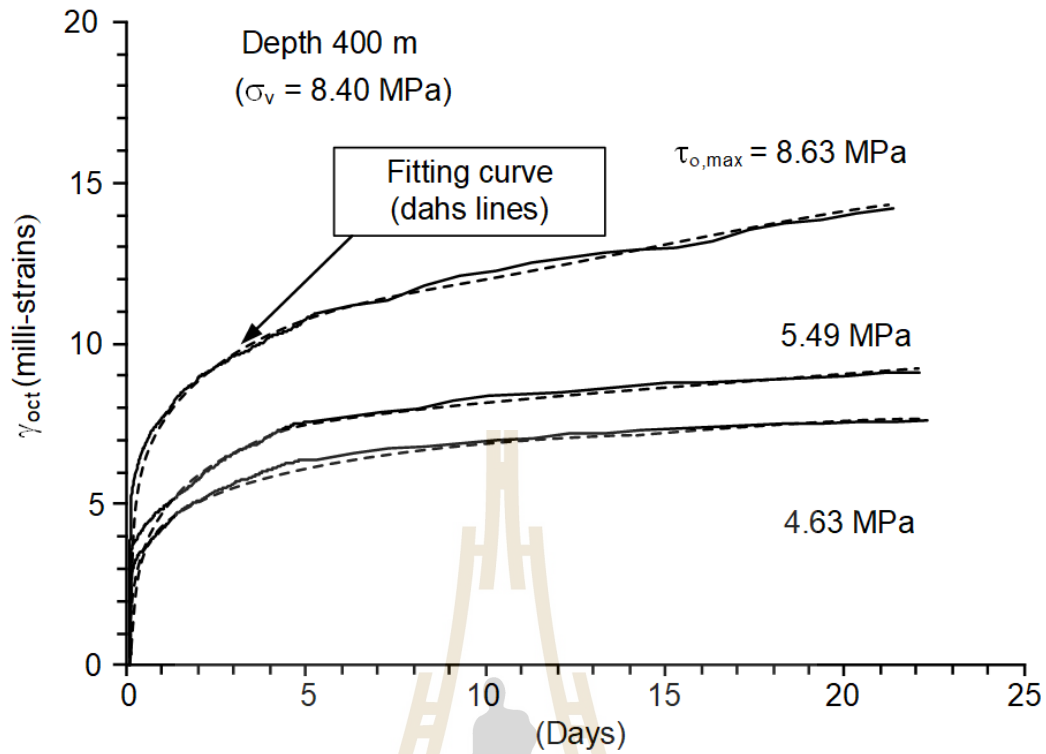


Figure 5.9 Octahedral shear strain as a function of time (solid lines) and curves fitting with Burgers model (dash lines) under octahedral shear stresses at depth 400 m.

Figure 5.10 plots the Burgers parameters as a function of the applied maximum octahedral shear stress. The diagrams also give the empirical equations to fit with the test results. The exponential equation seems to show the best description for the Burgers parameters and time relations. It seems that the creep deformations under instantaneous and transient phases (E_1 , E_2 , η_2) are not sensitive to the changes of the maximum octahedral shear stress ($\tau_{oct,max}$). The visco-plastic coefficient (η_1) reflecting the steady-state creep phase, however, tends to decrease with increasing the shear stress. This observation agrees with those of Fuenkajorn and Phueakphum (2010) who performed cyclic loading tests on Maha Sarakham salt under unconfined condition.

Table 5.1 Calibration results of Burgers parameters.

Depth (m)	Extraction ratio (e)	Octahedral shear stress ($\tau_{oct,max}$)	Burgers Parameters				
			E_1 (GPa)	E_2 (GPa)	η_1 (GPa·Day)	η_2 (GPa·Day)	R^2
250	30	2.89	2.60	2.48	92.41	1.79	0.966
	40	3.43	2.47	2.38	82.63	1.58	0.965
	60	5.40	2.19	2.07	62.20	1.59	0.947
300	30	3.47	2.48	2.42	95.39	1.66	0.962
	40	4.12	2.34	2.30	60.17	1.45	0.951
	60	6.47	2.46	2.60	55.14	1.54	0.926
350	30	4.05	2.26	2.10	70.55	1.41	0.950
	40	4.80	2.46	2.34	64.05	1.57	0.916
	60	7.55	2.47	2.40	58.62	1.51	0.935
400	30	4.63	2.28	2.20	60.44	1.72	0.944
	40	5.49	2.26	2.16	49.01	1.86	0.946
	60	8.63	2.29	2.32	40.36	1.41	0.958

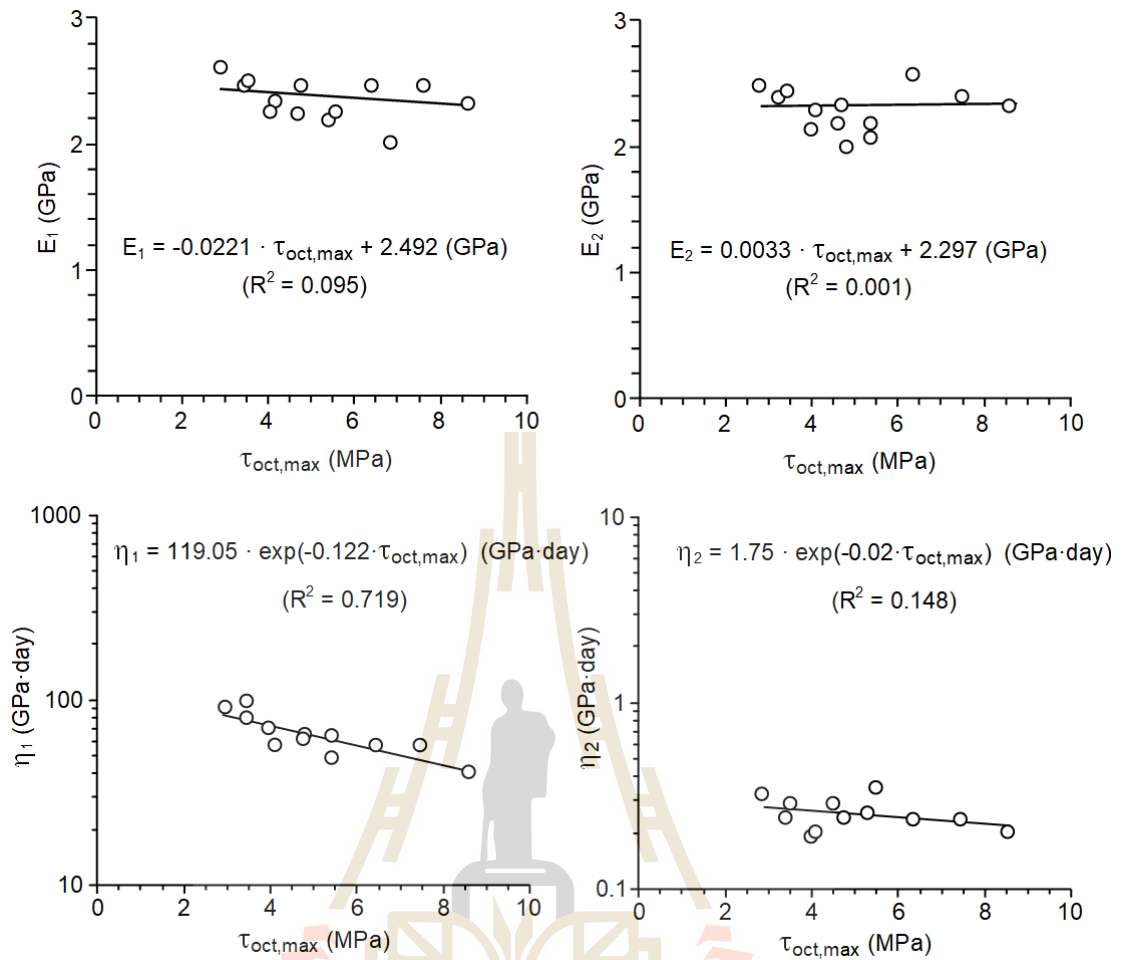


Figure 5.10 Burgers parameters as a function of maximum octahedral shear stress.

5.3.2 Potential creep law

The potential law has long been used to describe the time-dependent behavior of rock salt (Fuenkajorn and Daemen, 1988). The potential law is power equation relating creep strain, stress and time. The total strain can be divided into two parts, elastic strain (linear and recoverable strain) and plastic creep strain (time-dependent and nonrecoverable strain) which can be expressed as:

$$[\varepsilon^T] = [\varepsilon^e] + [\varepsilon^c] \quad (5.5)$$

where ε^T is vector of total strain, ε^e is elastic strain and ε^c is plastic creep strain

To consider both axial and lateral creep strains, the octahedral shear stresses and strains during static and cyclic loadings are determined using the following relations (Jaeger et al, 2007):

$$\tau_{\text{oct,max}} = \frac{\sqrt{2}}{3} \cdot (\sigma_1 - \sigma_3) \quad (5.6)$$

$$\gamma_{\text{oct}} = \frac{\sqrt{2}}{3} \cdot (\varepsilon_1 - \varepsilon_3) \quad (5.7)$$

where $\tau_{\text{oct,max}}$ are maximum octahedral shear stresses calculated under withdrawal conditions, σ_1 and σ_3 with are the major and minor principal stresses, γ_{oct} is the octahedral shear strain, and ε_1 and ε_3 are the measured axial and lateral strains.

The total, elastic and plastic creep strain in terms of the octahedral shear strain can be written as:

$$[\gamma_{\text{oct}}^T] = [\gamma_{\text{oct}}^e] + [\gamma_{\text{oct}}^c] \quad (5.8)$$

where $[\gamma_{\text{oct}}^T]$, $[\gamma_{\text{oct}}^e]$ and $[\gamma_{\text{oct}}^c]$ are three-dimensional vectors of total, elastic and time-dependent strains.

The elastic strain from the test results can be obtained from the constant octahedral shear stress and shear modulus (G) (Jaeger et al, 2007):

$$\gamma_{\text{oct}}^e = \tau_{\text{oct,max}} / 2G \quad (5.9)$$

The potential creep law can present the creep behavior of salt in terms of the octahedral shear stress and octahedral shear strain as a function of time.

$$\gamma_{\text{oct}}^c = \kappa \cdot \tau_{\text{oct,max}}^\beta \cdot t^\gamma \quad (5.10)$$

where κ , β and γ are material parameters. Substituting equations (5.9) and (5.10) into (5.11) the total octahedral shear strain can be presented as a function of testing time, octahedral shear stress and plastic creep strain:

$$\gamma_{\text{oct}}(t) = (\tau_{\text{oct,max}}/2G) + (\kappa \cdot \tau_{\text{oct,max}}^\beta t^\gamma) \quad (5.11)$$

The shear modulus can be obtained from relatively quick unloading as those performed by Luangthip et al. (2017) on the same rock salt. They define G as 7.84 GPa

Regression analyses on the octahedral shear strain-time curves based on the SPSS statistical software are performed to determine the creep parameters for each specimen. Figures 5.11 through 5.14 show the calibration results. They are presented by dash lines. The calibrated parameters for combined static and cyclic results are $\kappa = 5.36 \text{ 1/MPa}\cdot\text{s}$, $\beta = 1.26$ and $\gamma = 0.16$ with $R^2 > 0.9$. Table 5.2 shows the potential law parameters calibrated from the experimental data. Table 5.3 compares the potential creep parameters from cyclic loading with those of the static loading by Wilalak and Fuenkajorn, (2016). The results indicate that the parameter κ obtained from cyclic loading test is higher than that of the static loading test, suggesting that the time dependent deformation tends to be softer and more sensitive to time when it is under cyclic loading.

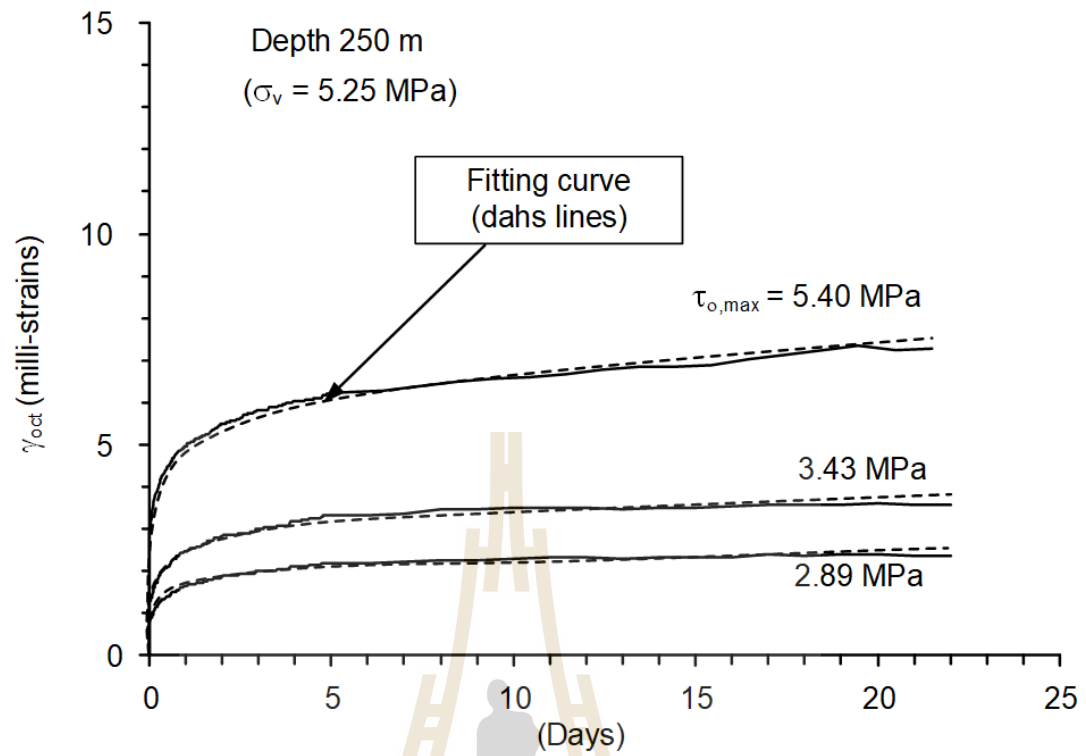


Figure 5.11 Octahedral shear strain as a function of time (solid lines) and curves fitting with potential law (dash lines) at depth 250 m.

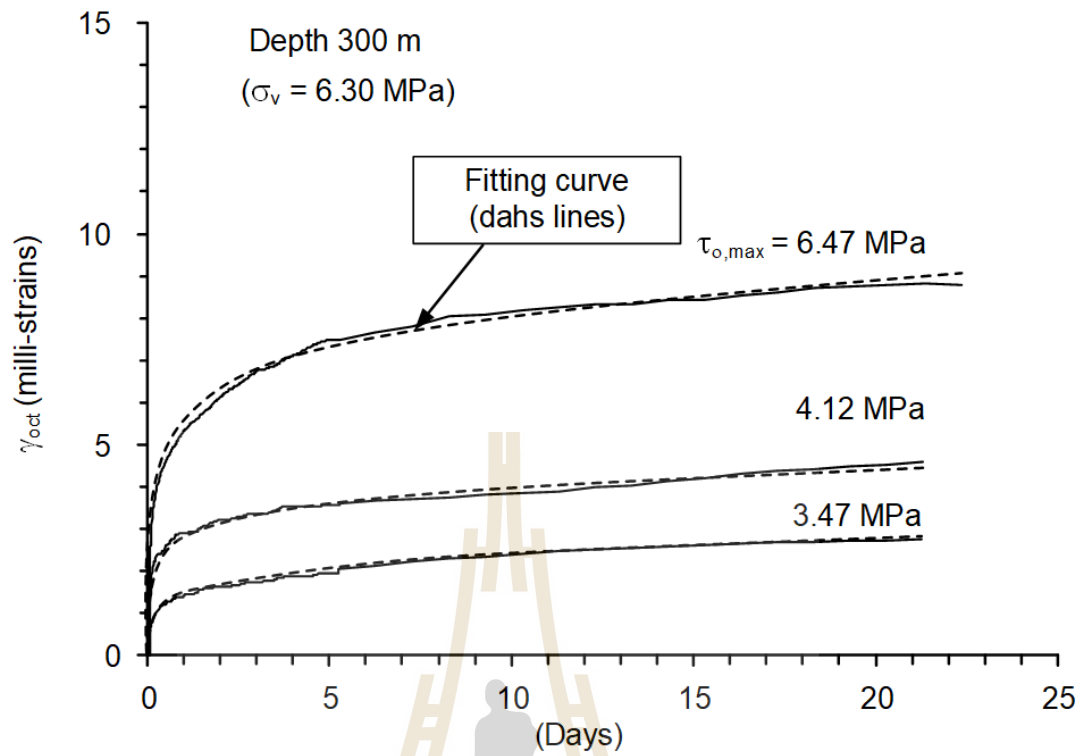


Figure 5.12 Octahedral shear strain as a function of time (solid lines) and curves fitting with potential law (dash lines) at depth 300 m.

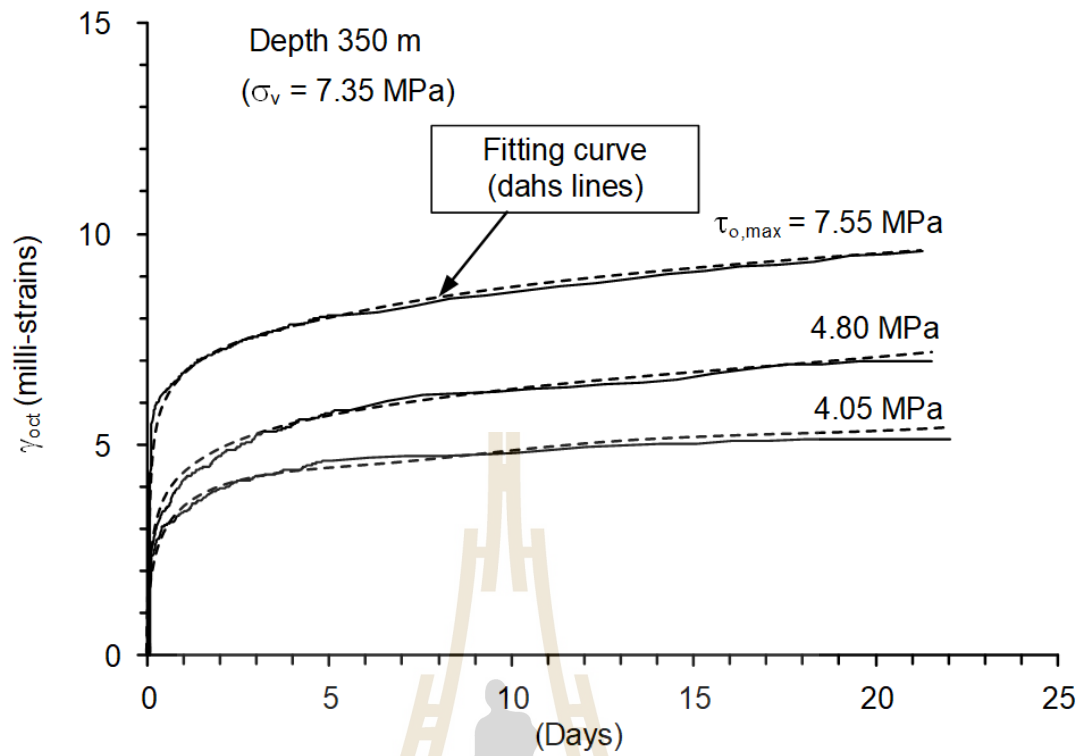


Figure 5.13 Octahedral shear strain as a function of time (solid lines) and curves fitting with potential law (dash lines) at depth 350 m.

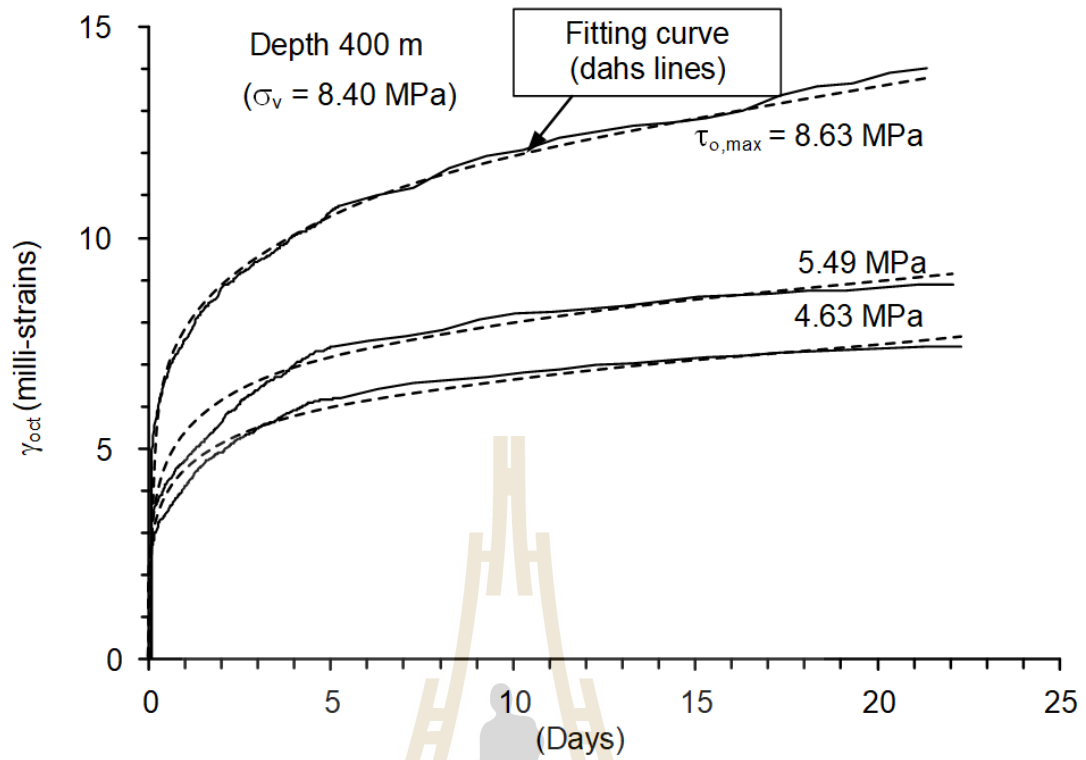


Figure 5.14 Octahedral shear strain as a function of time (solid lines) and curves fitting with potential law (dash lines) at depth 400 m.

Table 5.2 Calibration results of Potential law parameters.

Depth (m)	Extraction ratio (e)	Octahedral shear stress $\tau_{oct,max}$ (MPa)	Potential Parameters			
			κ ($\times 10^9/MPa \cdot s$)	β	γ	R^2
250	30	2.89	5.54	1.25	0.16	0.970
	40	3.43	5.34	1.26	0.17	0.973
	60	5.40	6.11	1.28	0.17	0.987
300	30	3.47	3.32	1.23	0.17	0.986
	40	4.12	5.07	1.23	0.16	0.973
	60	6.47	5.17	1.22	0.16	0.988
350	30	4.05	5.76	1.27	0.15	0.973
	40	4.80	5.69	1.27	0.16	0.987
	60	7.55	5.23	1.25	0.14	0.930
400	30	4.63	6.13	1.26	0.17	0.979
	40	5.49	5.85	1.26	0.19	0.975
	60	8.63	5.18	1.28	0.19	0.982
Mean \pm SD			5.26 \pm 0.73	1.26 \pm 0.02	0.16 \pm 0.01	

Table 5.3 Creep parameter of static and cyclic loading.

Creep parameters	Static loading for Wilalak and Fuenkajorn, (2016)	Cyclic loading
κ ($\times 10^9/MPa \cdot s$)	2.97	5.26
β	1.37	1.26
γ	0.19	0.16

CHAPTER VI

TIME-DEPENDENT STRENGTH OF SALT

UNDER CYCLIC LOADING

6.1 Introduction

An attempt is made here to predict the compressive strength of rock salt after subjecting to repeated cycles of loading and unloading under triaxial stress states. Recognizing the fact that the creep testing performed here is relatively short-term, none of the specimen has reached tertiary creep phase or failure, time-dependent strengths of the salt are needed to predict the stability of salt pillars under long-term storage operation. This can be achieved by determine the strain energy accumulated by the specimens during cyclic loadings. The calculated strain energy can be compared with the maximum strain energy (at failure) obtained by other research on the same Maha Sarakham salt. Described in this chapter includes calibration of the strain energy density for each specimen, application of creep model to obtain the stress-strain and time relations, and comparison of the calculated strain energy against the maximum energy that Maha Sarakham salt can sustain before failure occurs.

6.2 Strain energy density calculation

The strain energy density principle is applied to describe the long-term strength of salt for use in the pillar design under different shear stresses and depths.

The distortional strain energy can be calculated from the octahedral shear stresses and strains for each specimen using the following relation (Jaeger et al., 2007):

$$W_d = (3/2) \cdot \tau_{\text{oct,max}} \cdot \gamma_{\text{oct}} \quad (6.1)$$

where $\tau_{\text{oct,max}}$ is maximum octahedral shear stresses during withdrawal period for each cycles and γ_{oct} is octahedral shear strains.

The distortional strain energy as a function of mean stress at failure ($W_{d,f}$) is adopted from experimental results supported by Junthong et al. (2016), as shown in Figure 6.1. The strains and their corresponding times at which the failure occurs can be determined by comparing the distortional strain energy obtained here with the strain energy criterion of rock salt at failure developed by Junthong et al. (2016). The mean stress (σ_m) can be calculated from axial stress and confining pressure for each salt specimen using the following relations:

$$\sigma_m = (\sigma_{1,\text{with}} + 2\sigma_{3,\text{with}})/3 \quad (6.2)$$

where $\sigma_{1,\text{with}}$ and $\sigma_{3,\text{with}}$ is axial stresses and confining pressure calculated under withdrawal condition.

The relations of $W_{d,f}$ - σ_m from Junthong et al. (2016) can be represented by a linear relation to exhibit the time-dependent strength of the salt. The distortional strain energy criterion can be empirically presented as a function of mean stress as follows:

$$W_{d,f} = (0.030) \cdot \sigma_m + 0.081 \quad (6.3)$$

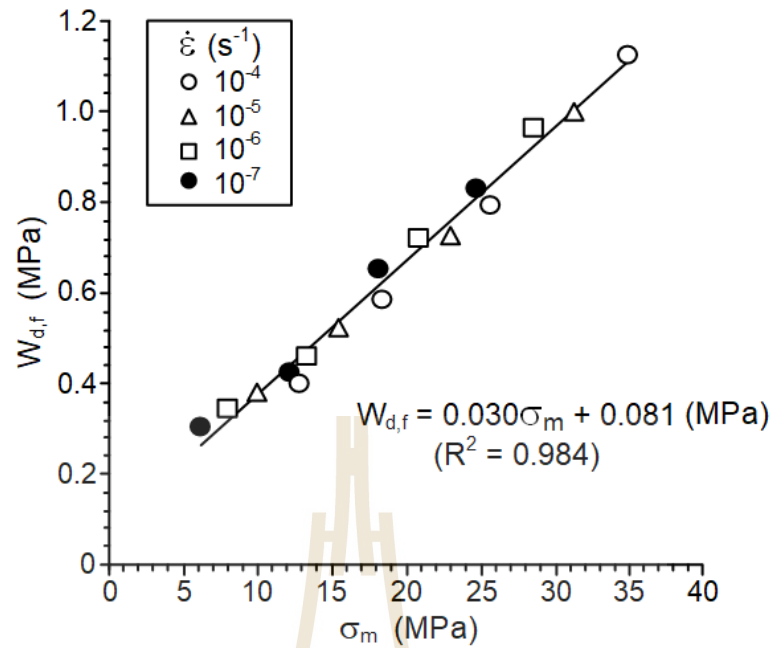


Figure 6.1 Distortional strain energy ($W_{d,f}$) at failure as a function of mean stress (σ_m) by Junthong et al. (2016).

6.3 Long-term salt strength based on potential law

In order to describe the increase of the strain with time under the triaxial cyclic loading condition, the potential creep law has been used. The octahedral shear strains as a function of time for potential law can be written as follows (Nair and Boreisi, 1970):

$$\gamma_{oct}(t) = (\tau_{oct,max}/2G) + (\kappa \cdot \tau_{oct,max}^\beta t^\nu) \quad (6.4)$$

The distortional strain energy can be calculated by substituting equations (6.4) into (6.1), and hence the following equation can be obtained:

$$W_d = (3/2 \cdot \tau_{oct,max}) \cdot [(\tau_{oct,max}/2G) + (\kappa \cdot \tau_{oct,max}^\beta t^\nu)] \quad (6.5)$$

By substituting the material parameters (Table 5.3) G , κ , β and γ in to equation (6.4) a series of octahedral shear strains time curves of salt under various depths and octahedral shear stresses (equivalent extraction ratios) can be developed. Figures 6.2 through 6.5 show the distortional strain energy as a function of testing time. The strains and their corresponding time at failure can be determined by comparing the distortional strain energy obtained here with the distortional strain energy criterion of rock salt at failure presented by Junthong et al. (2016) (Figure 6.1). The factor of safety (FS) can be determined with relation to time, depth and extraction ratio.

$$FS = W_{d,f}/W_d \quad (6.6)$$

where $W_{d,f}$ is the distortional strain energy criterion given by Junthong et al. (2016), W_d is the distortional strain energy calculated from the test results. For factor of safety equal to 1.0 ($W_d = W_{d,f}$), the time at which the salt reaches their failure points can be determined by:

$$t = [[(2W_{d,f}/3\tau_{oct,max}) - (\tau_{oct,max} / 2G)] / (\kappa\tau_{oct,max} \beta)]^{1/\gamma} \quad (6.7)$$

Figure 6.6 shows the time at failure calculated for depths from 150 to 400 m and assuming extraction ratios from 30% to 60% (represented by $\tau_{oct,max}$). The results suggest that the duration under stable condition decreases with increasing extraction ratios and depths. These diagrams can be used as a guideline to ensure that the salt pillars will remain stable during compressed-air energy storage. The diagrams in Figure 6.6 show that the salt can deform more quickly under cyclic loading than under static

loading. The durations before failure occurs for depths of 150 to 400 m and extraction ratio from 30% to 60% are shown in Tables 6.1.

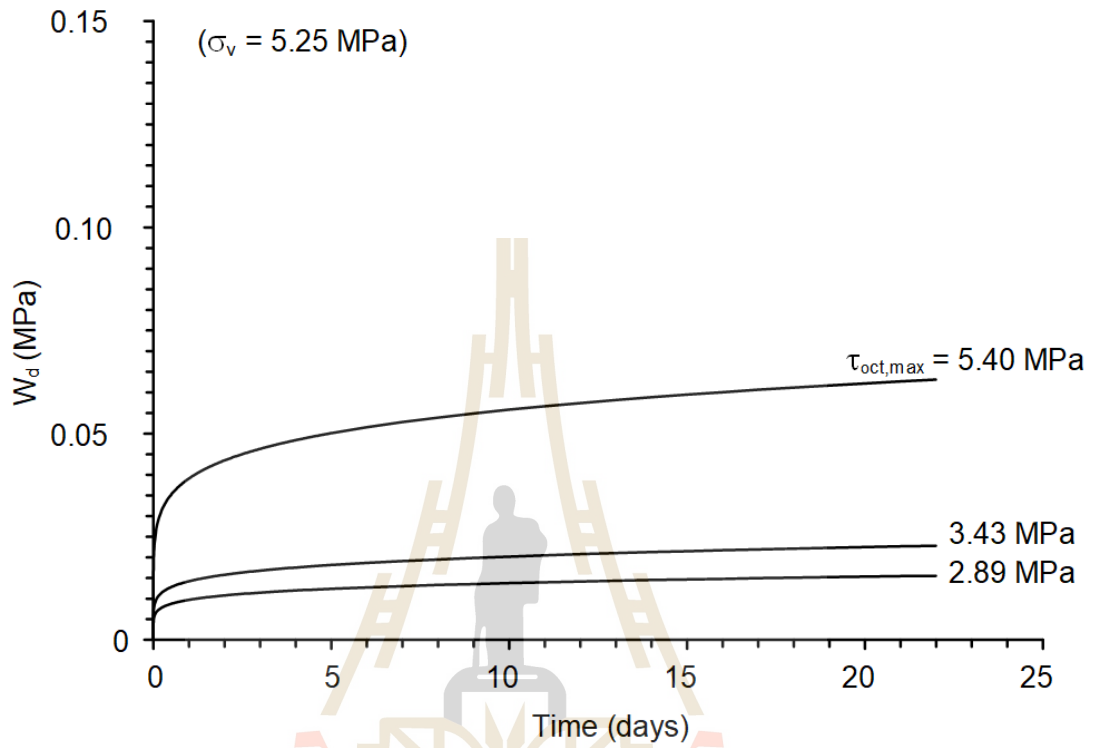


Figure 6.2 Calculated distortional strain energy as a function of testing time based on potential law for depth of 250 m.

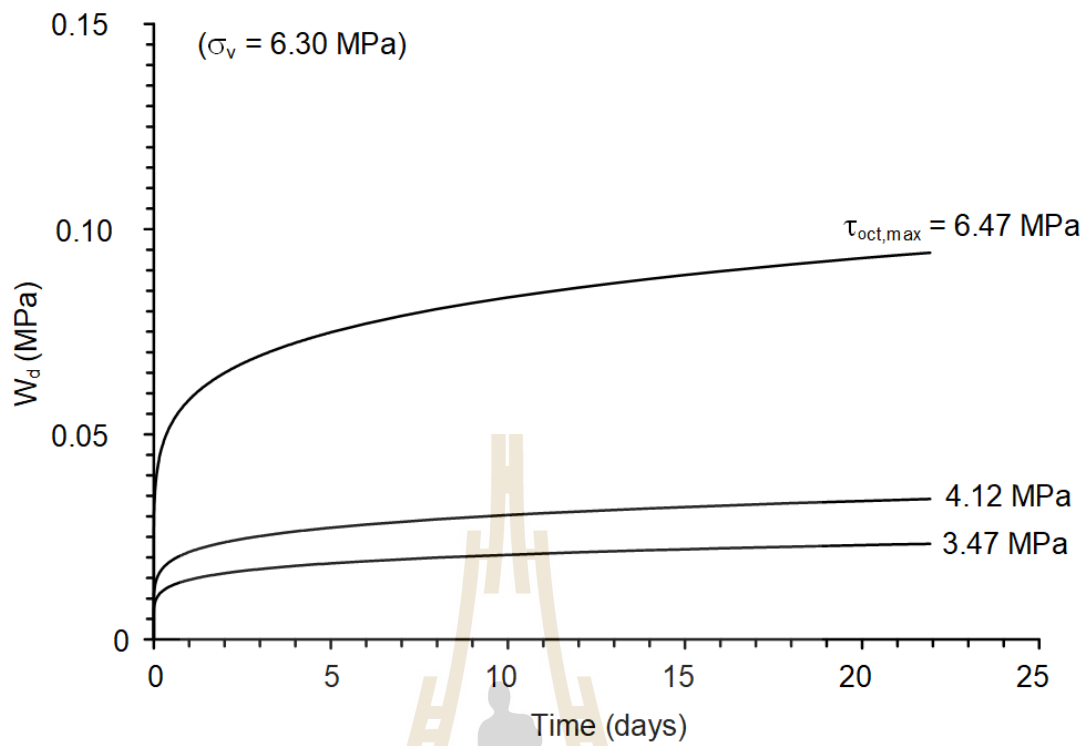


Figure 6.3 Calculated distortional strain energy as a function of testing time based on potential law for depth of 300 m.

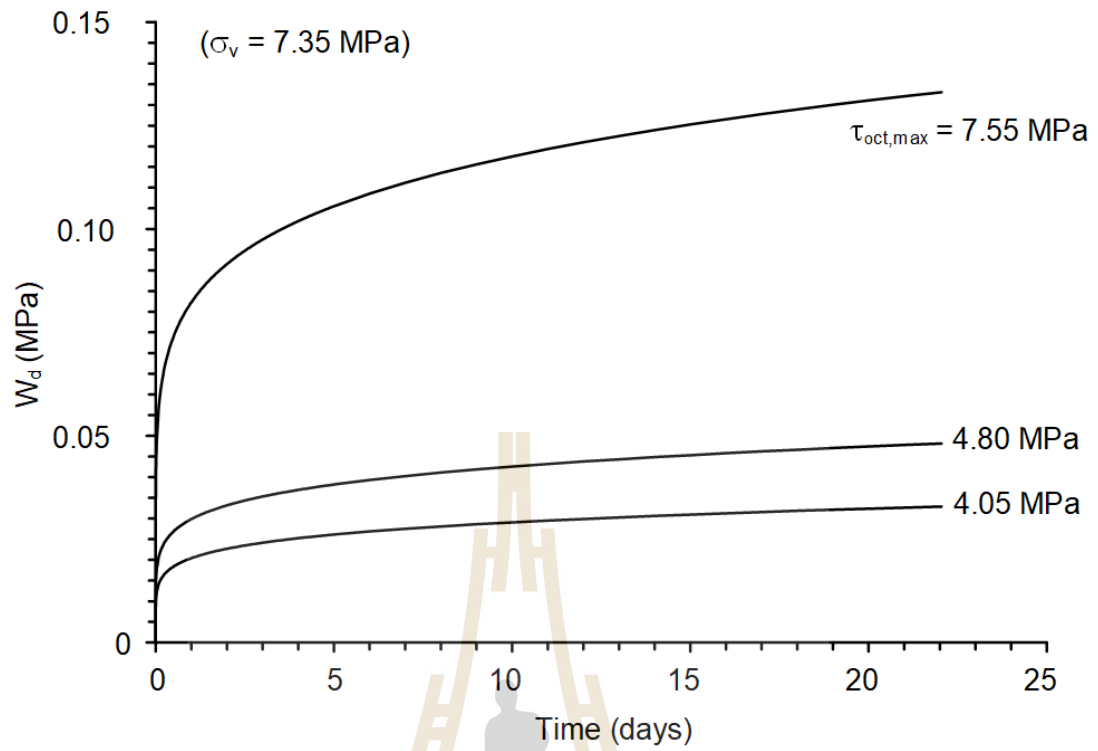


Figure 6.4 Calculated distortional strain energy as a function of testing time based on potential law for depth of 350 m.

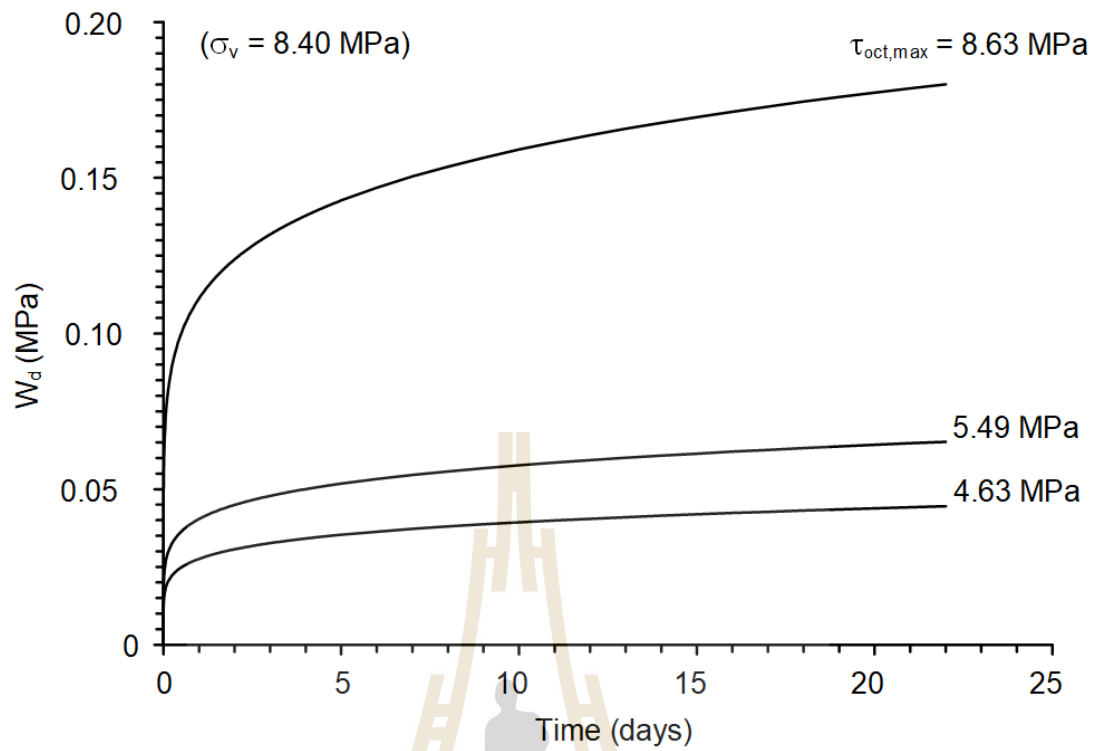


Figure 6.5 Calculated distortional strain energy as a function of testing time based on potential law for depth of 400 m.

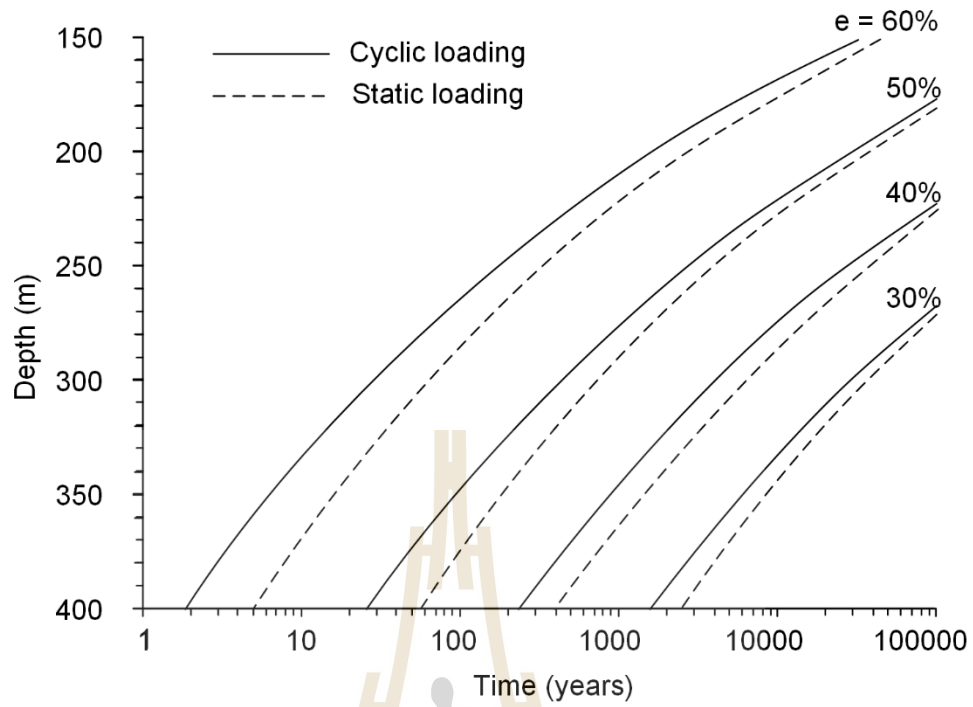


Figure 6.6 Prediction of time at failure based on potential law, comparing static (dash lines) with cyclic (solid lines) loading conditions.

Table 6.1 Predictions of time at which failure occurs based on potential law.

Depth (m)	Extraction ratio, e (%)	Time at failure (years)	
		Static loading	Cyclic loading
150	30	51.4×10^6	36.7×10^6
	40	6.54×10^6	5.53×10^6
	50	6.06×10^5	5.89×10^5
	60	4.34×10^4	3.36×10^4
200	30	2.11×10^6	1.93×10^6
	40	3.03×10^5	2.82×10^5
	50	3.50×10^4	2.70×10^4
	60	2.68×10^3	2.68×10^3
250	30	2.11×10^5	1.93×10^5
	40	3.43×10^4	2.67×10^4
	50	4.11×10^3	2.67×10^3
	60	3.31×10^2	1.74×10^2
300	30	3.63×10^4	2.88×10^4
	40	6.04×10^3	4.11×10^3
	50	7.48×10^2	4.26×10^2
	60	6.24×10^1	2.90×10^1
350	30	8.47×10^3	5.98×10^3
	40	1.44×10^3	8.74×10^2
	50	1.82×10^2	9.33×10^1
	60	1.56×10^1	6.55
400	30	2.45×10^3	1.58×10^3
	40	4.24×10^2	2.35×10^2
	50	5.47×10^1	2.56×10^1
	60	4.80	1.84

6.4 Long-term salt strength based on Burgers model

Similar to the potential law application (described in section 6.3), the Burgers model can be used to calculate the octahedral shear strains as a function of time for each cyclic loading specimen. A governing equation of the Burgers model is adopted here (Fuenkajorn and Daemen, 1988):

$$\gamma_{\text{oct}}(t) = \tau_{\text{oct}} \left[\frac{1}{E_1} + \frac{t}{\eta_1} + \frac{1}{E_2} \left(1 - \exp\left(\frac{-E_2 t}{\eta_2} \right) \right) \right] \quad (6.8)$$

where E_1 and E_2 are the spring constants in instantaneous and transient phases, η_1 and η_2 are the viscosity coefficients in steady-state and transient phase. Distortional strain energy are obtained based on the Burgers model which can be calculated by substituting equations (6.8) into (6.1):

$$W_d = \left(\frac{3}{2} \cdot \tau_{\text{oct,max}} \right) \cdot \left[\tau_{\text{oct,max}} \cdot \left(\frac{1}{E_1} + \frac{t}{\eta_1} + \frac{1}{E_2} \left(1 - \exp\left(\frac{-E_2 t}{\eta_2} \right) \right) \right) \right] \quad (6.9)$$

Figures 6.7 through 6.10 show the distortional strain energy as a function of testing time. The duration at failure can also be predicted by using $FS = 1.0$, as shown in Figure 6.11. The results suggest that the duration under stable condition decreases with increasing extraction ratios and depths. The Burgers parameters can be determined for the static loading test data obtained by Wilalak et al. (2016). The results indicate that the viscosity coefficient in steady-state phase (η_1) obtained from static loading test is higher than that of the cyclic loading, suggesting that the salt tends to be less viscous

when it is under cyclic loading. The numerical values shown in Figures 6.7 through 6.10, are given in Table 6.3 for both cyclic and static loading conditions.

6.5 Comparisons of long-term salt strengths

Comparison of the maximum durations that the salt can sustain under triaxial cyclic loading between the potential law and Burgers model calculations suggests that there are significant discrepancies between the two models. Predictions based on Burgers model give notably more conservative results than those based on potential law. (i.e. comparing Figures 6.6 and 6.11). This may be due to the fact that Burgers model has a separated term to describe the steady-state creep phase (t/η_1), implying that the shear strains are accumulated steadily and relatively quickly during steady-state creep phase. The creep curves predicted by the potential law, however, exhibit that the strain rates reduce with increasing time. The difference of the predictions from the two models have been reported also by Wilalak and Fuenkajorn (2016) who performed static creep testing on the same rock salt.

Even though both models have been extensively used to describe the creep behavior of rock salt from various locations worldwide (Fuenkajorn and Daemen, 1988), conclusion model has not been drawn to indicate which can give more representation of the rheological properties of the salt. In the context of the study reported herein, both models can be applied to the actual storage operation, as a minimum, for the feasibility study state. The Burgers model can give the lower bound of the design, while the potential law provides the upper bound.

It is important to recognize that the time-dependent salt strengths under triaxial cyclic loading determined in this chapter dose not directly represent the pillar strengths.

There are numerous factors that are needed to consider in order to correlate the laboratory test results with the actual pillar design under in-situ conditions. These include, for example, pillar shapes, mechanical properties of salt roof and floor, and salt panel design. The pillar shape factors involve height-to-width ratio and length-to-width ratio. Both have significant impact on the stability of the pillars (Obert and Duvall, 1967). Short and wide pillars are stronger and stiffer than tall and narrow pillars, and definitely exhibit higher mechanical stability, as compared to laboratory test specimens. This is due to the effect of shape and length-to-diameter ratio (Jaeger et al., 2007).

Salt pillars supporting between strong roof and floor are likely more stable than those placed between soft roof and floor, as their top and bottom portions cannot be easily dilated in lateral directions. The top and bottom portions will subject to shearing resistance, and hence strengthens the pillars.

Due to the pillar design factors mentioned above, pillar design based on the tributary area concept may not be appropriate, as the obtained results would be overly-conservative. The applicability of the research findings obtained here nevertheless remains valid. For example, the predicted long-term salt strengths can be incorporated into a computer model that represents the actual pillar geometry and its boundary conditions. The loading in the simulation can be under static condition while using the creep parameters that have been calibrated under cyclic loading conditions.

Table 6.2 Burgers parameters for static and cyclic loadings.

Burgers parameters	Static loading for Wilalak et al. (2016)	Cyclic loading
E1 (GPa)	2.70	2.31
E2 (GPa)	2.11	2.50
η_1 (GPa.day)	120.0	70.0
η_2 (GPa.day)	1.80	1.60

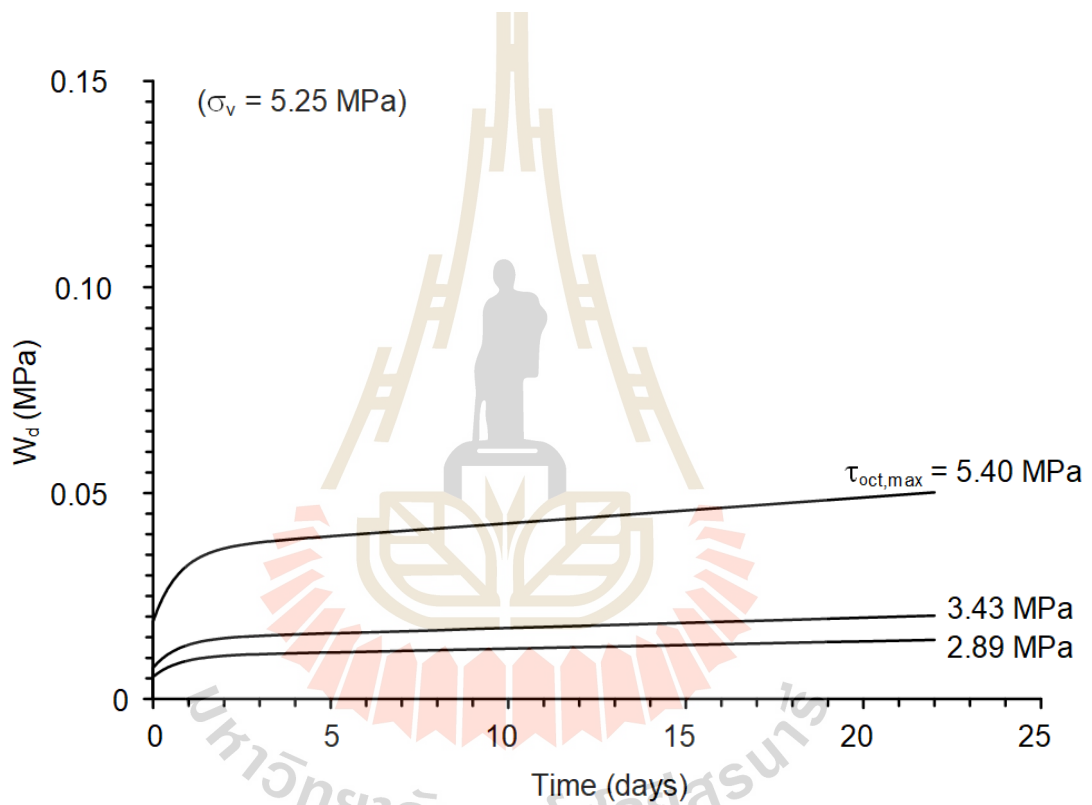


Figure 6.7 Calculated distortional strain energy as a function of testing time based on Burgers model for depth of 250 m.

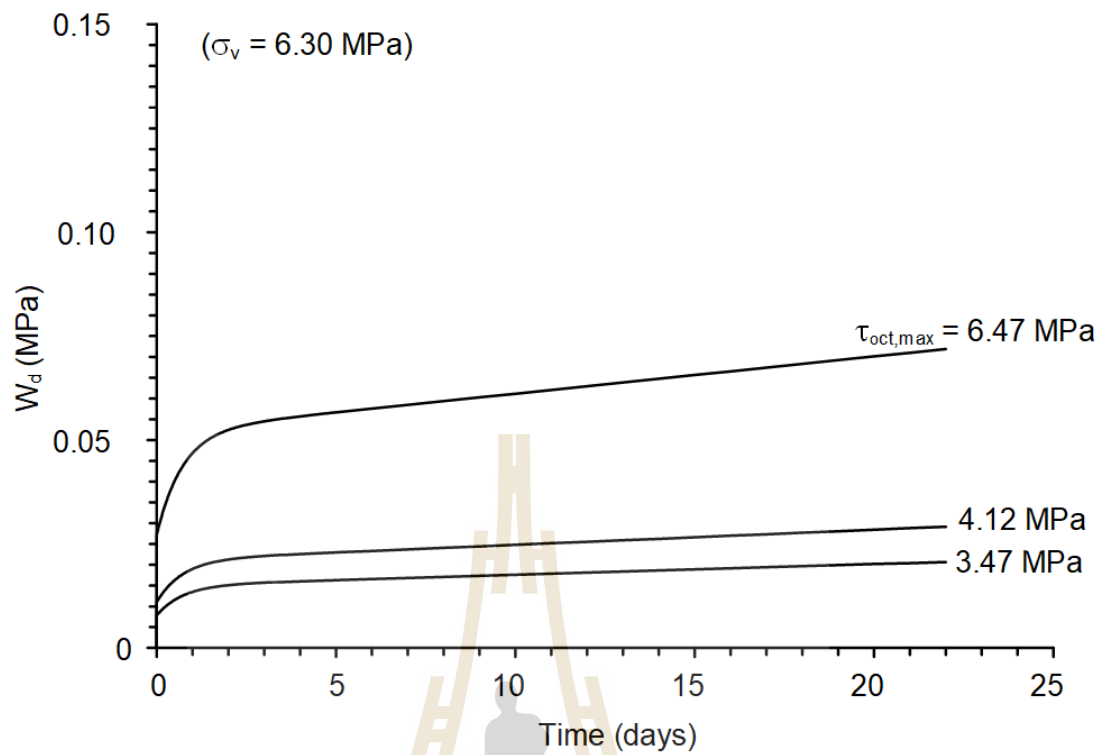


Figure 6.8 Calculated distortional strain energy as a function of testing time based on Burgers model for depth of 300 m.

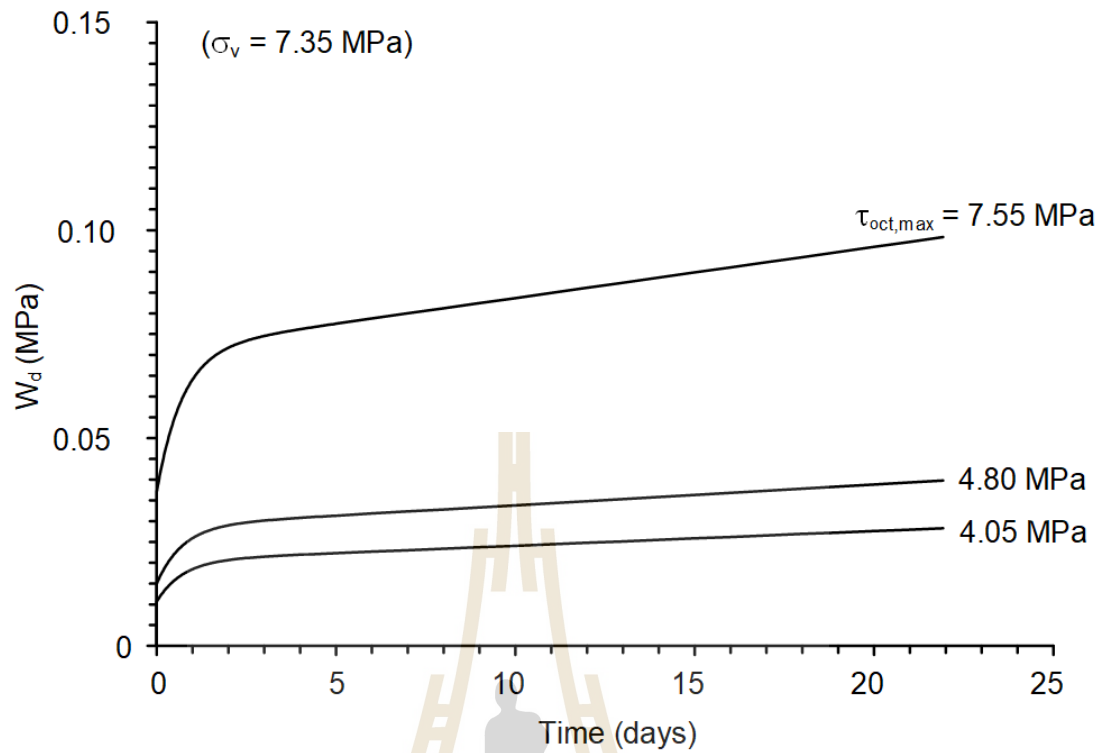


Figure 6.9 Calculated distortional strain energy as a function of testing time based on Burgers model for depth of 350 m.

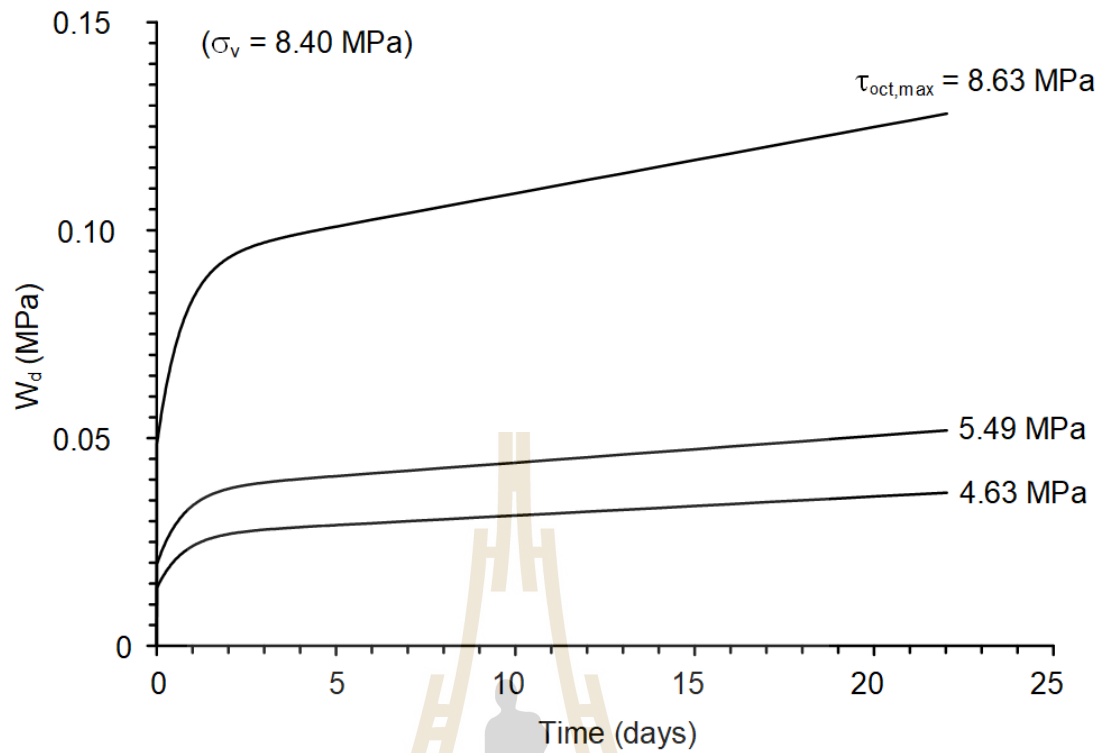


Figure 6.10 Calculated distortional strain energy as a function of testing time based on Burgers model for depth of 400 m.

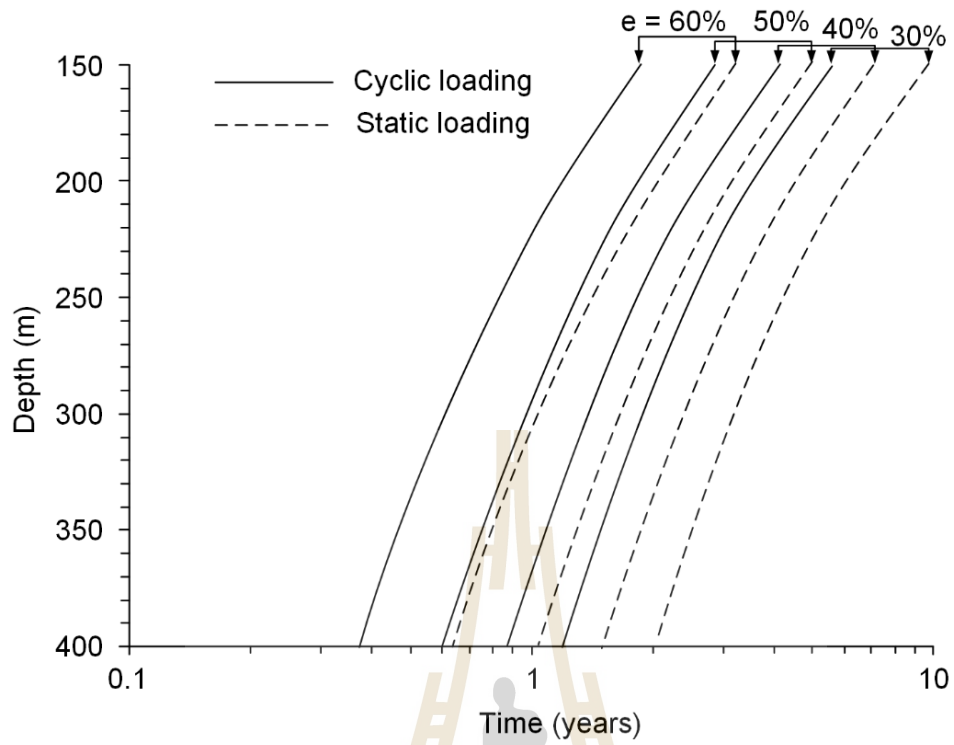


Figure 6.11 Predictions of time at failure based on Burgers model, comparing static (dash lines) with cyclic (solid lines) loading conditions.

Table 6.3 Predictions of time at failure occurs based on Burgers model.

Depth (m)	Extraction ratio, e (%)	Time at failure (years)	
		Static loading	Cyclic loading
150	30	9.60	5.60
	40	7.08	4.13
	50	4.95	2.89
	60	3.21	1.88
200	30	6.02	3.52
	40	4.46	2.60
	50	3.12	1.82
	60	2.02	1.18
250	30	4.23	2.47
	40	3.14	1.83
	50	2.19	1.28
	60	1.41	0.82
300	30	3.19	1.86
	40	2.36	1.38
	50	1.64	0.96
	60	1.04	0.61
350	30	2.51	1.47
	40	1.85	1.08
	50	1.28	0.75
	60	0.81	0.47
400	30	2.05	1.19
	40	1.50	0.88
	50	1.03	0.60
	60	0.64	0.37

CHAPTER VII

DISCUSSIONS AND CONCLUSIONS

7.1 Discussions

This section presents the issues relating to the reliability of the test methods and results, comparisons of the findings with those of researchers elsewhere, limitations and applicability of the knowledge obtained from this study.

The creep strains during static loading (first 5 days) and during cyclic loading (6th through 21st days) are reliable, as evidenced by that the magnitudes of the strains under higher octahedral shear stresses and equivalent extraction ratios are larger than those under the lower ones. Correct are also the fluctuations of the strains during cyclic loading. Larger fluctuations are observed from the larger stress amplitudes (differences between the $\tau_{\text{oct,max}}$ and $\tau_{\text{oct,min}}$). The observed slight discrepancies are probably caused by the intrinsic variability of the specimens (i.e., in terms of non-uniform distributions of inclusions, grain sizes and grain boundary orientations with respect to the main loading axis).

Admittedly, only one specimen has been tested under each set of test parameters (e.g. equivalent extraction ratio, $\tau_{\text{oct,max}}$, depth). More specimens tested under the same set of parameters would provide a redundant result and a more rigorous calibration of the model parameters. Nevertheless, the present results of 12 specimens representing four depths and three equivalent extraction ratios ($\tau_{\text{oct,max}}$) satisfactorily show promising findings, particularly in terms of the visco-plastic strains (during steady-state creep

phase) which are all higher than those obtained elsewhere under static loadings under the same applied shear stresses. The selected depth ranges between 250 and 400 m and the equivalent extraction ratios between 30% and 60% represent those that are currently applied by salt and potash mining industry both in the Sakon Nakhon and Khorat basins. The selections are primarily aimed at utilizing the abandoned salt openings or panels from these mines.

The total test durations of 21 days (5 days under static loads and 16 days under cyclic loads) seem adequate, as evidenced by a clear trend of the plastic strains obtained under all sets of test parameters. Unless the specimens reach failure, application of a longer test period would not provide any more benefit toward this study. The test periods used here also provide the strain results that fit well to both Burgers model and potential creep law, exhibiting R^2 greater than 0.9 for all specimens. The axial and lateral strains measured during cyclic loading show small visco-elastic strains after both reloading and unloading. This suggests that even though the salt is undergone plastic creep deformation, it still poses small elastic and visco-elastic properties. The magnitudes of the recoverable strains after unloading are much smaller than those measured at the beginning of testing (instantaneous strain). This does not support the postulation given by many researchers (e.g., Jaeger et al., 2007; and Fuenkajorn and Daemen, 1988) that the strain recovered after unloading would be equal to the instantaneous strain obtained from the beginning of the test. The small elastic and visco-elastic responses observed here agree with those observed by Archeeploha and Fuenkajorn (2013) who conduct cyclic loading on the same Maha Sarakham salt. The discrepancies between the predictions obtained from the Burgers model and the potential creep law clearly suggest that a more comprehensive constitutive model needs

to be developed. Even though both models give good correlations with the strain-time data, significant deviation is observed when they are extrapolated to describe long-term behavior of the salt. The new constitutive model should be able to incorporate the healing mechanism of the induced microcracks which would likely occurs in salt even when it is subjected to a constant deviatoric (shear) stress. With the incorporation of the time-dependent healing term that has been calibrated from test data such as those obtained by (Charoenpiew, 2015), the constitutive equation would be more complete, and the long-term creep strain rate would be reduced, and hence its predictions would be more realities.

Applicability of the research finding toward the actual compressed-air energy storage operation in a mine panel may not be possible at this time. It should be noted that there are several components and factors that are needed to study and understand. Notably mentioned here include, for example, roof conditions, mine panel and abutment (barrier) design, potential product leakage through crack and fractures induced during excavation, fluctuation of temperatures during inject and retrieval periods, and effect of humidity of the external air on the creep deformation of the host salt boundaries. It is true that some of these factors has been individually investigated in the laboratory, particularly on the Maha Sarakham salt. For example, the effect of temperatures has been studied by Phatthaisong et al. (2016) under compression and by Wisetsaen et al. (2015) under tension. The salt roof would probably be the most vulnerable components for underground storage in salt mines. Kaewpuang et al. (2018) have investigated the effect of cyclic compression-to-tension loading on the salt beams and found that tensile strengths of salt under compression-to-tension cyclic loading is

only half of these under tension cyclic loading and about one fourth of those under static loading (e.g., Brazilian tensile strength).

The panel configurations are important factor dictating the vertical stress on the salt pillars depending also the overall extraction ratio. Note that the equivalent extraction ratio used in this study is for individual support pillars. Under in-situ mine panel, the stress on the pillar is likely much less than the ones are here. This is due to the fact that most of the vertical stresses are imposed on the abutment (barrier) pillars. Such configurations are sometimes called stress arc or stress trajectory (Serata et al., 1989). How much stresses are distributed on a pillar depend largely on the panel design (widths of abutment pillars, support pillars and of panel itself). In summary, the application of the tributary area concept used here would be overly conservative compared to the actual mine panel configurations. If the vertical and pillar stresses (σ_v and σ_p) used here are conservative, the axial strains obtained from the testing would also be larger than the actual as well.

The issue of product leakage bypasses any seal or bulkhead has been studied in the laboratory and under in-situ conditions by Stormont and Daemen (1991) Their results strongly indicate that excavation-induced damage zone at the opening boundary of salt can become significant preferential flow path of stored product. Higher product (here is compressed-air) pressure, higher flow rate of leakage will occur.

In the light of the issues mentioned above, simulations of the actual compressed-air storage in mine panel remain extremely difficulty, if not impossible. As most researches, even those from overseas, have investigated numerically or experimentally on individual factor or factors that could affect the long-term stability of the storage facility in salt. Nevertheless, the experimental effort performed here has never been

attempted elsewhere. The findings obtained here clearly provide a precursory step toward the actual storage operation.

Finally, it should be noted that the designed stress states imposed on salt specimens are intentionally under constant mean stress (σ_m). Such stress design would likely represent those under actual storage operation. More important, it provides a conservative result, with regards to the measured strains, as compared to other relevant researcher that used constant confining stress (σ_3) configurations. Figure 7.1 compares the visco-plastic coefficient η_1 , obtained here (constant σ_m) with those obtained by Archeeploha and Fuenkajorn (2013) who performed cyclic loading on Maha Sarakham salt under constant σ_3 . It is clear that the visco-plastic coefficients obtained under constant σ_m are about 20 GPa.day lower than those under constant σ_3 .

7.2 Conclusions

Triaxial cyclic loading under constant mean stresses has been performed on Maha Sarakham salt specimens with nominal dimensions of $54 \times 54 \times 108 \text{ mm}^3$. The applied stress schemes are designed to simulate the salt pillars immediately after excavation under static loads for 5 days. The subsequent cyclic stresses are applied for 16 days (16 cycles). The stress amplitudes are dictated by the differences between the 90% and the 20% of the vertical stresses at a considered depth. They are determined in terms of the maximum and minimum air pressures (P_{\max} and P_{\min}) around the salt pillars which are equivalent to the calculated maximum and minimum octahedral shear stresses ($\tau_{\text{oct,max}}$ and $\tau_{\text{oct,min}}$) in the salt specimens. Twelve specimens have been tested by subjecting to twelve cyclic shear stress amplitudes (four depths by three equivalent

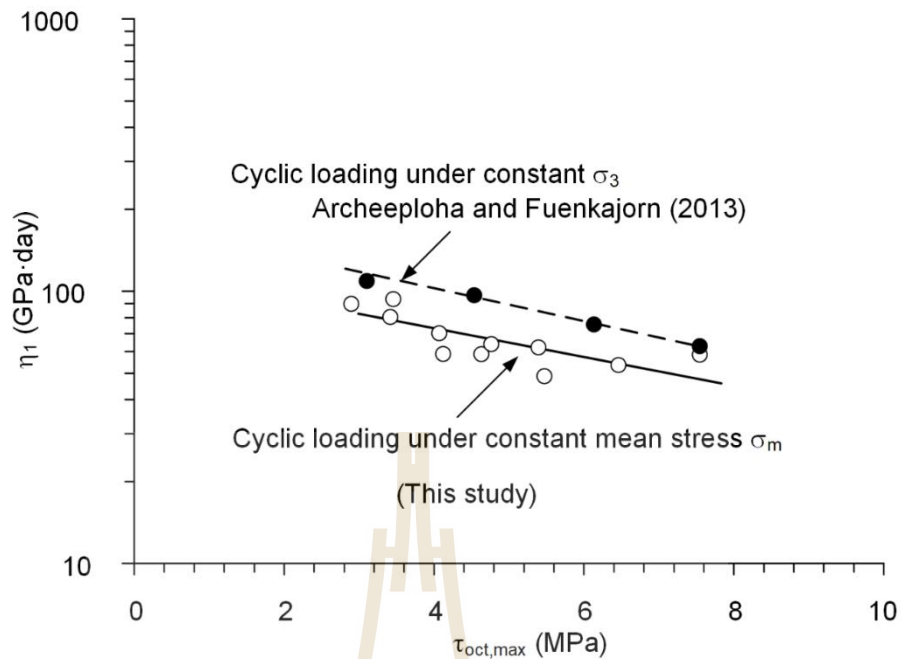


Figure 7.1 Comparison of η_1 calibrated from cyclic loading with constant σ_3 by Archeeploha and Fuenkajorn (2013) and from constant σ_m used in this study.

extraction ratio). The measured octahedral shear strains-time curves for all specimens fit well to the Burgers model and potential creep law ($R^2 > 0.9$). Their parameters are used to extrapolate the plastic strains beyond the test duration used here. Strain energy densities of the creep results are calculated and compared with the maximum strain energy (at failure) obtained from relevant research to determine the time at which failure occurs for each set of the test parameters.

Conclusion drawn from this study can be summarized as follows.

- 1) The γ_{oct} -time curves measured during static and cyclic loadings show that higher strain rates and magnitudes are obtained under higher applied octahedral shear stresses. In another word, the strain rates and magnitudes will increase with the simulated depths, vertical stresses and equivalent extraction ratios.

2) The shear stress amplitudes induce the fluctuations of the octahedral shear strains measured during cyclic loading. For each specimen, the difference of the maximum and minimum induced strains tends to remain constant with time or with the number of loading cycles.

3) The degrees of the strain fluctuation or strain amplitudes increase with the simulated depths and equivalent extraction ratios.

4) The Burgers model and potential creep law fit well to the $\gamma_{\text{oct-t}}$ curves drawn from the loci of the maximum induced strains of each loading cycle under maximum shear stress (equivalent to P_{min} during withdrawal period).

5) The shear strain-time curves obtained under cyclic loading here exhibit larger magnitudes and rates, as compared to those under static loading obtained elsewhere on the same Maha Sarakham salt.

6) The visco-plastic strains (η_1) in the steady-state creep phase obtained from cyclic loading under constant mean stresses are about 20 GPa.day lower than those under constant confining stress obtained elsewhere. The constant mean stress condition is similar to those of the actual underground storage facility in rock salt.

7) The strain energy-time relation is developed to compare with the maximum strain energy that salt can sustain (obtained from relevant research elsewhere) for both creep models. Both models show that the factors of safety of salt reduce with increasing depths and extraction ratios.

8) For long-term prediction, the Burgers model accumulates plastic creep strain much quicker than does the potential creep law. As a result, the Burgers model provides a much more conservative analysis and failure prediction than the potential creep law.

7.3 Recommendations for future studies

Shortcomings and limitations of the applicability of the results obtained from this study lead to the following recommendations for immediate future studies.

1) Larger salt specimens should be tested under cyclic loading. The minimum sizes would preferably be 10 cm in diameter. This could minimize the dislocation glide mechanism and enhance the dislocation climb mechanism (Senseny, 1984). As a result, the steady-state creep strain rates would be reduced, and hence provides laboratory results that are closer to the actual large size salt pillars.

2) Constitutive equation that can incorporate the healing mechanism and thermal effect should be developed. Admittedly, such mathematical relations would be highly complex and require exhaustive test data to calibrate their parameters.

3) Larger numbers of tested specimens are desirable to minimize the intrinsic variability of the salt specimens.

4) An actual mine panel configurations may be used to determine the pillar stress, instead of using the tributary area concept. This would make the test results more realistic and more site-specific.

5) Cyclic loading under stresses and periods (interval cyclic loading) as performed here may be expanded for different intervals. For example, the injection and withdrawal periods may be increased from 12 hours periods to one or two days periods. Results obtained under different loading frequencies would reveal different mechanical responses of the salt which could be benefit toward the design and analysis of the actual storage operation.

REFERENCES

- Allemandou, X. and Dusseault, M. B. (1996). Procedures for cyclic creep testing of salt rock, results and discussions. In **Proceedings of the Third Conference on the Mechanical Behavior of Salt** (pp. 207-218). Clausthal-Zellerfeld, Germany: Trans Tech Publications.
- Archeeploha, S. and Fuenkajorn, K. (2013). Effects of cyclic loading on creep behavior of Maha Sarakham salt. In **Proceedings of the Fourth Thailand Symposium on Rock Mechanics** (pp. 91-98). Nakhon Ratchasima, Thailand.
- ASTM D4543. **Standard Practice for Preparing Rock Core Specimens and Determining Dimensional and Shape Tolerances**. Annual Book of ASTM Standards (Vol. 04.08). Philadelphia.
- Atterwell, P. B. and Farmer, I. W. (1973). Fatigue behavior of rock. **International Journal of Rock Mechanics and Mining Sciences**. 10: 1-9.
- Burdine, N. T. (1963). Rock failure under dynamic loading conditions. **Society of Petroleum Engineers Journal**. 3(1): 1-8.
- Crotogino, F., Mohmeyer, W. U., and Scharf, R. (2001). Huntorf CAES: More than 20 years of successful operation. In **Proceedings of the Solution Mining Research Institute (SMRI) Spring Meeting** (pp. 351-362). Florida, USA.
- Change, G. C., Thompson, P. A., Allen, R. A., and Loscutoff, W. V. (1980). Underground compressed air energy storage for electric utilities. **Subsurface**. 2: 579-585.

- Cristescu, N. and Hunsche, U. (1996). A comprehensive constitutive equation for rock salt determination and application. In **Proceedings of the Third Conference on the Mechanical Behavior of Salt** (pp. 191-205). Clausthal-Zellerfeld, Germany: Trans Tech Publications.
- Charoenpiew, P. (2015). Laboratory study of healing effectiveness of salt fracture under normal stress and temperatures. **Master Thesis**. Suranaree University of Technology, Nakhonratchasima, Thailand.
- DeLong, M. M., Nelson, C. R., and Petersen, D. L. (1989). Subsurface cavern system requirements for compressed air energy storage and associated uses. In Nilsen & Olsen (eds.). **Storage of Gases in Rock Caverns** (ISBN 906191 896 0, pp. 33-36). Balkema, Rotterdam.
- EPRI (1986). **Dynamic Operating Benefits of Energy Storage**. EPRI Report No.AP-4875, Palo Alto, CA, Electric Power Research Institute.
- EPRI (1990a). **Compressed Air Storage for Electric Power Generation**. EPRI Report No.GS-6784, Palo Alto, CA, Electric Power Research Institute.
- EPRI (1990b). **Compressed-Air Energy Storage using Hard-Rock Geology**. Palo Alto, CA, Electric Power Research Institute.
- EPRI (1990c). **Rock Concern Linings for Compressed-Air Energy Storage**. Palo Alto, CA, Electric Power Research Institute.
- EPRI (1992a). **Alabama Electric Cooperative (AEC) Builds First U.S. Compressed Air Energy Storage (CASE) Plant Using EPRI-Developed Low-Pressure Expander**. EPRI Report No.IN-101511, Palo Alto, CA, Electric Power Research Institute.

- EPRI (1992b). **CASE goes on-line [Video recording]**. Palo Alto, CA, Electric Power Research Institute.
- EPRI (1992c). **EPRI-Developed Acquisition System Monitors Compressed-Air Energy Storage CAES Plant On-line Performance**. EPRI Report No.IN-101510, Palo Alto, CA, Electric Power Research Institute.
- EPRI (1994a). **Compressed Air Handbook**. EPRI Report No. CR-104546, Palo Alto, CA, Electric Power Research Institute.
- EPRI (1994b). **Compressive Analyses of Compressed–Air Cycles; CASE, CASE-ES, CRCAES/CRCASH-ES, and MRCAES/MRCASH-ES**. EPRI Report No.TR-103521, Palo Alto, CA, Electric Power Research Institute.
- EPRI (1994c) **Development of Turbomachinery Trains for the CASHING, NGCASH, and IGCASH Cycle Applications**. EPRI Report No.TR-103348, Palo Alto, CA, Electric Power Research Institute.
- EPRI (1994d). **Standard Compressed-Air Energy Storage Plant: Design and Cost**. Research Project No. TR-103209, Palo Alto, CA, Electric Power Research Institute.
- EPRI (1997). **Energy Storage in a Restructured Electric Utility Industry: Report on EPRI Think Tanks I and II**. EPRI Report No.TR-108894, Palo Alto, CA, Electric Power Research Institute.
- EPRI (1999). **Conceptual Engineering and Cost Estimate for 100-MW and 20MW Nominal Capacity CASH Plants**. EPRI Report No.TR-113360, Palo Alto, CA, Electric Power Research Institute.

- Fuenkajorn, K. and Daemen, J. J. K. (1992). Borehole sealing, Compressed-Air Energy Storage. In **Proceedings of the Second International Conference** (pp. 5.1-5.21). San Francisco, California.
- Fuenkajorn, K. and Daemen, J. J. K. (1988). **Boreholes Closure in Salt**. Technical Report Prepared for The U.S. Nuclear Regulatory Commission. Report No. NUREG/CR-5243 RW. University of Arizona.
- Fuenkajorn, K. and Phueakphum, D. (2010). Effects of cyclic loading on mechanical properties of Maha Sarakham salt. **Engineering Geology**. 112 (1-4): 43-52.
- Fuenkajorn, K, Sriapai, T., and Samsri, P. (2012). Effects of loading rate on strength and deformability of Maha Sarakham salt. **Engineering Geology**. 135-136: 10-23.
- Fuenkajorn, K. and Serata, S. (1992). Geohydrological integrity of CAES in rock salt. In **Proceedings of the Second International Conference on Compressed-Air Energy Storage** (pp. 4.1-4.21). San Francisco, California.
- Farmer, I.W. and Gilbert, M.J. (1984). Time dependent strength reduction of rock salt. In **Proceedings of the First Conference on the Mechanical Behavior of Salt** (pp. 3-18). Clausthal-Zellerfeld, Germany.
- Findley, W.N., Lai, J.S., and Onaran, K. (1989). **Creep and Relaxation of Nonlinear Viscoelastic Material: With an Introduction to Linear Viscoelasticity**. North-Holland, New York. 371 pp.
- Gehle, R. M. and Thoms, R. L. (1986). **Test of U.S. rock salt for long-term stability of CAES reservoir**. Richland, Washington: Pacific Northwest Laboratory.
- Hedley, D.G.F. (1967). An appraisal of convergence measurements in salt mines. In **Proceedings of the Fourth Canadian Rock Mechanics Symposium** (pp.117-135). Ottawa: Mines Branch, Dept. of Mines and Technical Surveys.

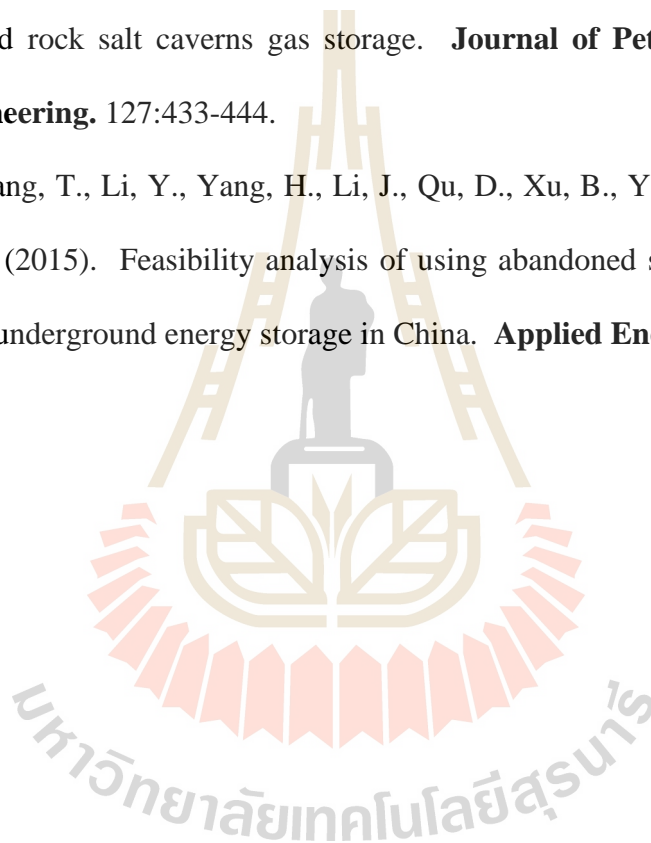
- Haimson, B. C. and Kim, C. M. (1972). Mechanical Behavior of rock under cyclic fatigue. In **Proceedings of the Thirteenth Symposium on Rock Mechanics** (pp.845-864). Urbana, Illinois.
- Haimson, B. C. (1972). **Mechanical Behavior of Rock under Cyclic Fatigue**. Annual Technical Report to the Bureau of Mines, Contract H0210004.
- Hardy, H. R. and Chugh, Y. P. (1970). Failure of geological materials under low-cycle fatigue. In **Proceedings of the Sixth Canadian Symposium on Rock mechanics** (pp.33-47). Montreal.
- Hamami, M., Tijani, S. M., and Vouille, G. (1996). A methodology for the identification of rock salt behavior using multi-step creep tests. In **Proceedings of the Third Conference on the Mechanical Behavior of Salt** (pp. 53-66). Clausthal-Zellerfeld, Germany: Trans Tech Publications.
- Hoek, E. and Brown, E.T. (1980). Empirical strength criterion for rock masses. **Journal of Geotechnical and Geoenvironmental Engineering**. 160(GT9): 1013-1035.
- Ishizuka, Y. and Able, T. (1990). Fatigue behavior of granite under cyclic loading. In Brummer (eds). **Static and Dynamics Consideration in Rock Engineering** (ISBN 90 6191 1453 2, pp.139-156). Rotterdam: Balkema.
- Junthong, P., Tepnarong, P., Artkhonghan, K., and Fuenkajorn, K., (2016). Prediction of time-dependent strengths of salt pillars using strain energy principle, **Research and Development Journal of the Engineering Institute of Thailand**. 27(4): 27-35.
- Jaeger, J. C., Cook, N. G. W., and Zimmerman, R. W. (2007). **Fundamentals of Rock Mechanics**. Blackwell publishing, Oxford.

- Kaewpuang, T., Plangklang, J, Khamrat, S., and Fuenkajorn, K. (2018). Effect of cyclic on tensile strength of rock salt. In **Proceedings of the Twelfth South East Asia Technical University Consortium Symposium (SEATUC)**. University Gadjah Mada, Yogyakarta, Indonesia.
- Katz, D. L. and Lady, E. R. (1976). **Compressed Air Storage**, Ann Arbor, Michigan: Ulrich's Book.
- Kim, C. M. (1973). Fatigue failure of rock in cyclic uniaxial compression. **PhD. Thesis**. University of Wisconsin, Madison
- Luangthip, A., Wilalak, N., Thongprapha, T., and Fuenkajorn, K. (2017). Effects of carnallite content on mechanical properties of Maha Sarakham rock salt. **Arabian Journal of Geosciences**. 10(149): 1-14.
- Ma, L.J., Liu, X.Y., Wang, M.Y., Xu, H.F., Hua, R.P., Fan, P.X., Jiang, S.R., Wang, G.A., and Yi, Q.K. (2013) Experimental investigation of the mechanical properties of rock salt under triaxial cyclic loading. **International Journal of Rock Mechanics & Mining Sciences**. 62: 31-41.
- Mogi, K. (1962). Study of elastic shocks caused by the fracture of heterogeneous materials and its relation to earthquake problem. **Bulletin of the Earthquake Research Institute**. 40: 125-173.
- Nair, K. and Boresi, A. (1970). Stress analysis for time-dependent problems in rock mechanics. In **Proceedings of the Second Congress of the International Society for Rock Mechanics** (pp. 531-536). Belgrade, Serbia.
- Obert, L. and Duvall, W. I. (1967). Rock mechanics and the design of structures in rock. **Journal of the Franklin Institute**. New York.

- Passaris, E. K. S. (1982). Fatigue characteristics of rock salt with reference to underground storage cavern. In **Proceedings of the ISRM Symposium** (pp. 983-989). Aachen, Germany.
- Plangklang, J., Artkhonghan, K., Tepnarong, P., and Fuenkajorn, K. (2017) Time-dependent tensile strength of Maha Sarakham salt. **Research and Development Journal of the Engineering Institute of Thailand**. 28(4): 5-12.
- Phatthaisong, k., Sartkaew, S., and Fuenkajorn, K. (2016) Effects of loading rate and temperature on strength and deformability of Maha Sarakham salt. **Songklanakarinn Journal of Science and Technology**. 40(2): 359-366.
- Roberts, L.A., Buchholz, S.A., Mellegard, K.D., and Dusterloh, U. (2015). Cyclic loading effects on the creep and dilation of salt rock. **Rock Mechanics and Rock Engineering**. 48: 2581–2590.
- Serata, S., Mehta, B., and Hiremath, M. (1989). Geomechanical stability analysis for CAES cavern operation. In Nilsen and Olsen (eds). **Storage of Gases in Rock Caverns** (pp. 129-135). Balkema, Rotterdam.
- Stormont, J. C. and Daemen, J. J. (1991). **Laboratory Study of Gas Permeability Changes in Rock Salt During Deformation**, SAND90-2638. Sandia National Laboratories, Albuquerque, NM. (p. 40).
- Song, R., Yue-ming, B., Jing-Peng, Z., De-yi, J., and Chum-he, Y. (2013). Experimental investigation of the fatigue properties of salt rock. **International Journal of Rock Mechanics and Mining Sciences**. 64:68-72.
- Senseny, P. E. (1984). Specimen size and History effect on creep of salt. Mechanical Behavior of Salt I, In **Proceedings of the First Conference on the Mechanical Behavior of Salt** (pp. 369-379). Clausthal-Zellerfeld, Germany.

- Swift, G.M. and Reddish, D.J. (2005). Underground excavations in rock salt. **Geotechnical and Geological Engineering**, 23 (1): 17–42.
- Thoms, R. L., Nathany, M., and Gehle, R. (1980). Low-frequency cyclic loading effect in rock salt. In **Proceedings of the International Symposium for Subsurface Space** (pp. 755-761). Stockholm.
- Thoms, R. L. and Gehle, R. (1982). Experimental study of rock salt for compressed air energy storage. In **Proceedings of the ISRM Symposium** (pp. 991-1002). Aachen, Germany.
- Thoms, R. L. and Martinez, J. D. (1978). **Preliminary Long-term Stability Criteria for Compressed Air Energy Storage Caverns in salt Domes**. Prepared for Battelle Northwest Laboratories, Richland, Washington, Special Agreement B-54804-A-L, Prime Contact EY-76-C-06-1830, 84 pp. Institute for Environmental Studies, Louisiana State University, Baton Rouge, LA.
- Tharp, T. M. (1973). Behavior of three calcite rock under tensile cyclic loading. **Master Thesis**. University of Wisconsin, Madison.
- Wisetsaen, S., Walsri, C., and Fuenkajorn, K. (2015). Effects of loading rate and temperature on tensile strength and deformation of rock salt. **International Journal of Rock Mechanics and Mining Sciences**, 73: 10-14.
- Wittke, W., Pierau, B., and Schetelig, K. (1980). Planing of a compressed-air pumped-storage scheme at Vianden/Luxembourg. In **Proceedings of the International Symposium for Subsurface Space** (pp. 367-376). Stockholm.
- Wendai, L. (2000). **Regression Analysis, Linear Regression and Profit Regression, In 13 Chapters; SPSS for Windows: Statistical Analysis**. Publishing House of Electronics Industry, Beijing, China.

- Warren, J. (1999). **Evaporites: Their evolution and economics** (pp. 235-239). Philadelphia: Blackwell Science.
- Wilalak, N. and Fuenkajorn, K. (2016). Constitutive equation for creep closure of shaft and borehole in potash layers with varying carnallite contents. In **Proceeding of the Ninth Asian Rock Mechanics Symposium**. Bali, Indonesia.
- Wang, T., Yang, C., Yan, X., and Daemen, J.J.K. (2015). Allowable pillar width for bedded rock salt caverns gas storage. **Journal of Petroleum Science and Engineering**. 127:433-444.
- Yang, C., Wang, T., Li, Y., Yang, H., Li, J., Qu, D., Xu, B., Yang, Y., and Daemen, J.J.K. (2015). Feasibility analysis of using abandoned salt caverns for large-scale underground energy storage in China. **Applied Energy**. 137:467-481



BIOGRAPHY

Mr. Kittisak Tengpakwaen was born on August 13, 1991 in Nakhon Ratchasima, Thailand. He received his Bachelor's Degree in Engineering (Geological Engineering) from Suranaree University of Technology in 2015. For his post-graduate, he continued to study with degree of Doctor of Philosophy in the Geological Engineering Program, Institute of Engineering, Suranaree university of Technology. During graduation, 2015-2020, he was a part time worker in position of research assistant at the Geomechanics Research Unit, Institute of Engineering, Suranaree University of Technology.

